

AFAMRL-TR-80-67

**LEVEL** *II*



10  
BS

## **ANALYSIS OF VERTEBRAL STRESS DISTRIBUTIONS AND EJECTION-RELATED INJURY MECHANISMS**

*M. PLESHA  
T. BELYTSCHKO  
NORTHWESTERN UNIVERSITY  
EVANSTON, ILLINOIS 60201*

**FEBRUARY 1981**

**MAY 8 1981**

Approved for public release; distribution unlimited.

**AIR FORCE AEROSPACE MEDICAL RESEARCH LABORATORY  
AEROSPACE MEDICAL DIVISION  
AIR FORCE SYSTEMS COMMAND  
WRIGHT-PATTERSON AIR FORCE BASE, OHIO 45433**

81 5 07 041

AD A 098 639

DTIC FILE COPY

## NOTICES

When US Government drawings, specifications, or other data are used for any purpose other than a definitely related Government procurement operation, the Government thereby incurs no responsibility nor any obligation whatsoever, and the fact that the Government may have formulated, furnished, or in any way supplied the said drawings, specifications, or other data, is not to be regarded by implication or otherwise, as in any manner licensing the holder or any other person or corporation, or conveying any rights or permission to manufacture, use, or sell any patented invention that may in any way be related thereto.

Please do not request copies of this report from Air Force Aerospace Medical Research Laboratory. Additional copies may be purchased from:

National Technical Information Service  
5285 Port Royal Road  
Springfield, Virginia 22161

Federal Government agencies and their contractors registered with Defense Documentation Center should direct requests for copies of this report to:

Defense Documentation Center  
Cameron Station  
Alexandria, Virginia 22314

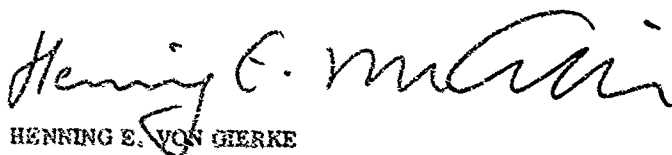
## TECHNICAL REVIEW AND APPROVAL

AFAMRL-TR-80-67

This report has been reviewed by the Office of Public Affairs (PA) and is releasable to the National Technical Information Service (NTIS). At NTIS, it will be available to the general public, including foreign nations.

This technical report has been reviewed and is approved for publication.

FOR THE COMMANDER



HENNING E. VON GIERKE  
Director

Biodynamics and Bioengineering Division  
Air Force Aerospace Medical Research Laboratory

SECURITY CLASSIFICATION OF THIS PAGE (When Data Entered)

19 REPORT DOCUMENTATION PAGE		READ INSTRUCTIONS BEFORE COMPLETING FORM	
1. REPORT NUMBER AFAMRL TR-80-67	2. GOVT ACCESSION NO. AD-A098539	3. RECIPIENT'S CATALOG NUMBER	
4. TITLE (and Subtitle) ANALYSIS OF VERTEBRAL STRESS DISTRIBUTIONS AND EJECTION-RELATED INJURY MECHANISMS		5. TYPE OF REPORT & PERIOD COVERED Final Technical Report Jul 1977-Jan 1980	
7. AUTHOR(s) M. Plesha T. Belytschko		8. CONTRACT OR GRANT NUMBER(s) F33615-77-C-0526	
9. PERFORMING ORGANIZATION NAME AND ADDRESS Department of Civil Engineering Northwestern University, Evanston, Illinois 60201		10. PROGRAM ELEMENT, PROJECT, TASK AREA & WORK UNIT NUMBERS 61102F, 2312-V3-03	
11. CONTROLLING OFFICE NAME AND ADDRESS Air Force Aerospace Medical Research Laboratory Air Force Aerospace Medical Division Wright-Patterson Air Force Base, Ohio 45433		12. REPORT DATE Feb 1981	
14. MONITORING AGENCY NAME & ADDRESS (if different from Controlling Office)		13. NUMBER OF PAGES 52	
		15. SECURITY CLASS. (of this report) UNCLASSIFIED	
		15a. DECLASSIFICATION/DOWNGRADING SCHEDULE	
16. DISTRIBUTION STATEMENT (of this Report) Approved for public release; distribution unlimited.			
17. DISTRIBUTION STATEMENT (of the abstract entered in Block 20, if different from Report)			
18. SUPPLEMENTARY NOTES			
19. KEY WORDS (Continue on reverse side if necessary and identify by block number) Biomechanics Stress Analysis Spine Impact			
20. ABSTRACT (Continue on reverse side if necessary and identify by block number) Stress analyses of lumbar vertebrae were performed by a three dimensional finite element method for the purposes of (1) evaluating simplified models of the vertebrae which are suitable as injury postprocessors, and (11) gaining a better understanding of injury mechanisms. The finite element analyses were linear and elastic. Axial and moment loads were applied over the end plates to simulate G <sub>z</sub> impact and on the facets to simulate load transmission between the articular facets and the vertebral bodies.			

DD FORM 1 JAN 73 1473

EDITION OF 1 NOV 65 IS OBSOLETE  
S/N 0102-014-6601

SECURITY CLASSIFICATION OF THIS PAGE (When Data Entered)

401292

The finite element model predicts that the maximum stresses under axial load are perpendicular to the axis of the vertebral body, which are called axial stresses; this is consistent with the predominance of compressive and wedge fractures. However, the maximum stresses predicted by the finite element model are only about a third of those predicted by the simplified injury model. This discrepancy is due to the fact that a substantial portion of the total load is transmitted through the vertebral centrum which is neglected in the simplified model. Furthermore, the finite element model exhibits a rather complex pattern of deformation even under axial load, which cannot be incorporated easily in a simplified model. The stresses predicted by the finite element model for bending also differ substantially from those given by the simplified model for the same reasons. Good agreement between the finite element model and simplified model is only achieved for torsion loads.

The difficulty does not lie in the geometry of the vertebral bodies. It was found that for axial loads or moments, the pedicles, variations in cortical bone thickness, and geometrical features such as taper had little effect on the stresses.

In the simplified models, the centrum was considered to be compressible. However, at high strain rates, fluid entrapment may lead to incompressible behavior of the centrum. The finite element models show that for an incompressible centrum, the maximum stresses are hoop stresses rather than axial stresses. This indicates a bursting mode of failure for high strain rates, which is in agreement with experimental findings.

The objective of the simplified models is to provide a measure of injury potential which can be used in conjunction with biodynamic models of the spine to predict the likelihood of injury in pilot ejection or other emergency flight procedures. However, these studies have shown that the stress magnitudes predicted by the simplified models are not consistent with the actual stress distributions because of the complexity of the load transmission in the vertebral body. To achieve reasonable consistency, either stress reduction factors based on finite element models or alternative simple models will need to be developed.

## PREFACE

This final technical report describes the work performed under Contract F33615-77-C-0526 from July 1, 1977 to January 30, 1980. The program was sponsored by the Air Force Aerospace Medical Research Laboratory, Aerospace Medical Division, Wright Patterson Air Force Base. The program monitor was Mr. Ints Kaleps of the Mathematics and Analysis Branch of the Biodynamics and Bioengineering Division.

Accession For	
NTIS GPO&I	<input checked="checked" type="checkbox"/>
DTIC TAB	<input type="checkbox"/>
Unannounced	<input type="checkbox"/>
Justification	
By	
Distribution/	
Availability Codes	
Avail and/or	
Dist	Special
A	

# TABLE OF CONTENTS

SECTION	Page
I INTRODUCTION	5
II ANATOMY AND INJURIES OF VERTEBRAE	7
III FINITE ELEMENT ANALYSIS	12
1. Finite Element Model	12
2. Axial Compression	15
1. Compressible Vertebral Centrum	15
2. Incompressible Vertebral Centrum	17
3. Comparison with Idealized Vertebral Model	21
3. Response to Bending Moment	21
1. Frontal Plane Moment	23
2. Sagittal Plane Moment	23
3. Torsion	26
IV REFINED FINITE ELEMENT MODELS	31
1. Effects of Small Changes in Cortical Bone Thickness	31
2. Finite Element Model 2 (Variable End Plate Thickness)	31
3. Finite Element Model 3 (Effects of Pedicle)	31
1. Axial Compression	33
2. Facet Load	33
V CONCLUSIONS	44
APPENDIX	46
REFERENCES	47

# LIST OF FIGURES

FIGURE		Page
1	Human vertebra.	8
2	Vertebral body fracture patterns resulting from spinal impact.	10
3	Vertebral models and stress nomenclature.	13
4	Finite element Model 1.	14
5	Deformed shapes of a vertebra subjected to various loads.	16
6	Trabecular bone principal stress directions for axial compression.	18
7	Cortical bone membrane stress profile; axial compression.	19
8	Cortical bone bending stress profile; axial compression.	20
9	Cortical bone membrane stress profile for an incompressible centrum; axial compression.	22
10	Cortical bone membrane stress profile; frontal plane bending.	24
11	Cortical bone bending stress profile; frontal plane bending.	25
12	Cortical bone membrane stress profile; sagittal plane bending.	27
13	Cortical bone bending stress profile; sagittal plane bending.	28
14	Cortical bone shear stress profile; axial torsion.	30
15	Finite element Model 3.	32
16	Anterior view of the cortical bone membrane stress profile; axial compression.	34
17	Posterior view of the cortical bone membrane stress profile; axial compression.	35
18	Frontal view of the cortical bone bending stress profile; axial compression.	36
19	Posterior view of the cortical bone bending stress profile; axial compression.	37
20	Frontal view of the cortical bone membrane stress profile; facet load.	39

LIST OF FIGURES (CONT.)

FIGURE		Page
21	Posterior view of the cortical bone membrane stress profile; facet load.	40
22	Illustration of elements used in load transfer analysis.	38
23	Frontal view of the cortical bone bending stress profile; facet load.	42
24	Posterior view of the cortical bone bending stress profile; facet load.	43



## SECTION I

### INTRODUCTION

In the last twenty years, numerous models have been developed for predicting the behavior of the spine during pilot ejection. Orne and Liu (1970) developed a two dimensional model which represented the vertebrae as rigid bodies interconnected by springs which represent the intervertebral discs and connective tissues. Belytschko et al (1976) subsequently developed a similar three dimensional model, which models the intervertebral discs by beam elements, and includes the effects of the articular facets. Material nonlinearities and large displacements of the spine were also treated. Prasad and King (1974) have considered two dimensional models which account for the facets. All of these models computed the forces and moments at the vertebral levels as functions of time.

An essential link in the application of these models to pilot safety during ejection is the interpretation of this output in terms of the likelihood of injury. The most serious category of injuries associated with pilot ejection are vertebral body fractures. Unfortunately, experimental data for vertebral body strength is not available for the numerous combinations of moments and axial forces which are pertinent to pilot ejection, and its determination would be prohibitively expensive. Therefore, it is desirable to relate the output of dynamic spine models to more basic variables, such as stresses in the vertebrae, for which experimental data is available.

The determination of the relationships between force levels and injury is a very difficult problem because many injury mechanisms are not well understood, the material properties are not well known, and there are considerable variations between individuals. Furthermore, for practicality in computations, the equations which relate model output to injury must be relatively simple.

As a first step towards this goal Belytschko et al (1976) proposed a vertebral model consisting of a cylindrical block enclosed by a cylindrical shell which represents the trabecular bone and the cortical bone, respectively. This, in conjunction with the assumption of uniform or linear strain distributions, yielded simple relationships between the forces and moments applied to the vertebrae and the resulting cortical bone stresses. By comparing the cortical bone stresses to experimentally determined strengths, the possibility of injury can be evaluated. However, this model neglects many important features of stress distribution, such as nonuniform strain distributions and incompressible behavior of the vertebral core.

In this report, more detailed stress analyses of vertebral

bodies are conducted to provide a better understanding of the stress distributions under applied axial load and moments. Three dimensional finite element models with linear material properties are used.

Finite element models have been previously applied to vertebral motion segments by Belytschko et al (1974), Kulak et al (1976) and Hakim and King (1979). The first two models were aimed primarily at the intervertebral discs. Hakim and King have used a three dimensional model to study stress distributions in a vertebra. Finite element analysis of other bones have been reported by Andriacchi et al (1976) and Tarr et al (1980).

## SECTION II

### ANATOMY AND INJURIES OF VERTEBRAE

In this section, the anatomy of lumbar vertebrae and the types of injuries encountered in emergency flight procedures are described.

A typical lumbar vertebra is shown in Fig. 1. Its major components are the vertebral body, the neural arch, the transverse and spinous processes and the articular facets.

The interior of the vertebral body is composed of cancellous (or trabecular) bone and also contains a substantial amount of fluid. It is encased circumferentially by a thin shell of cortical (compact) bone. The trabeculae of cancellous bone generally exhibit two well defined directions, axial and transverse. The axial trabeculae, which lie in the direction of axial loads, such as body weight, are thick and bound together by thinner transverse trabeculae. The structure contains numerous interstices which are filled with fluid.

The upper and lower surfaces of the vertebral body are thin plates of slightly porous, cortical bone, which are called end plates. Extending from each side of the vertebral body are bony projections called pedicles, which are connected to each other by the lamina. At the pedicle-lamina junctions, the superior articular processes project upward and the inferior articular processes project downward. The transverse processes extend laterally from the junctions; their structure is similar to that of the vertebral body, a core of soft bone encased by a thin shell of compact bone.

Each vertebra is connected to adjacent vertebrae through the intervertebral discs and the synovial joints at the articular processes. The intervertebral disc consists of three main parts: the nucleus pulposus in the center, the annulus fibrosus in the periphery, and the cartilage plates above and below. The annulus fibrosis in the adult lumbar spine is formed by a series of concentric lamellae, which consist of collagen fibers in two well defined axes of orientation. The nucleus is composed of nonorientated collagen fibers enmeshed in a mucoprotein gel. According to Duschel (1930), the water content of the nucleus ranges from 88% at birth to approximately 69% at age 77. In addition, numerous ligaments and muscles interconnect the vertebrae.

Kazarian (1975) has classified emergency flight procedure injuries as follows:

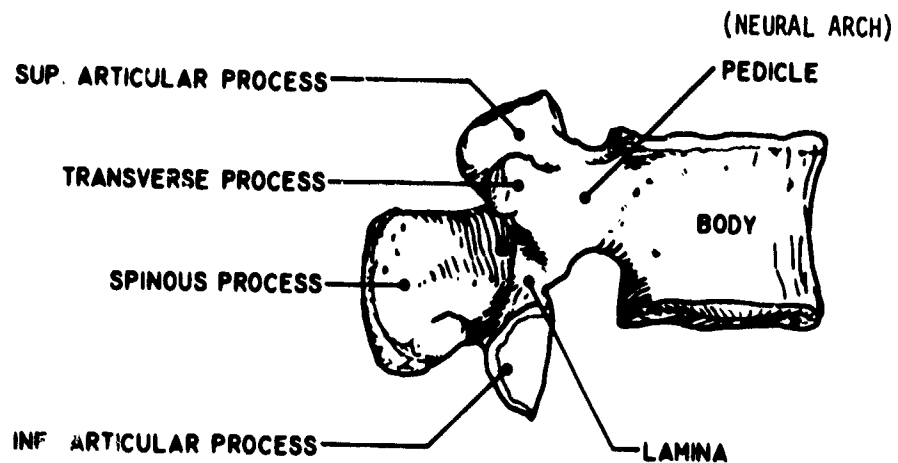
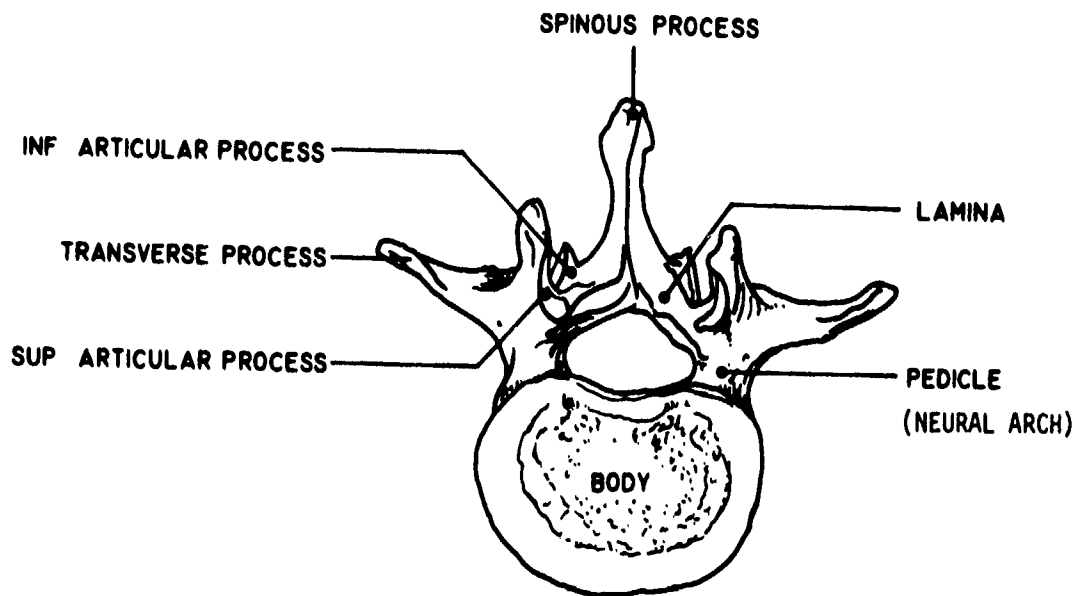


Figure 1. Human vertebra.

- compression fractures of the vertebral body
- radiologically concealed fractures
- fracture dislocations

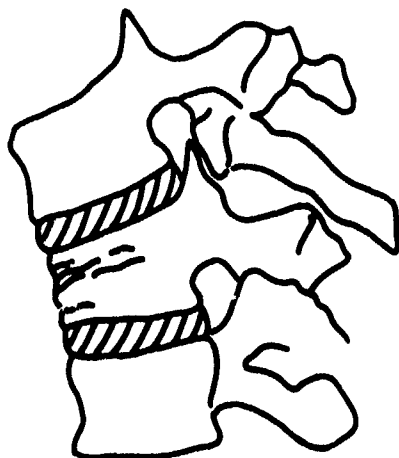
The first group includes all vertebral body fractures which do not involve the posterior of the vertebrae. It includes over 78% of all operational spinal injuries, so although these injuries are often not life-threatening, they are quite important.

Compression fractures occur in various patterns, such as anterior wedge fractures, lateral wedge fractures, and cleavage fractures. The major initiating mechanical factor in these injuries appears to be the compressive axial force sustained by the vertebral bodies. However, lateral and sagittal plane moments also appear to play a role, as indicated by the distinct appearance of anterior and lateral wedges. Some of these fractures are illustrated in Fig. 2.

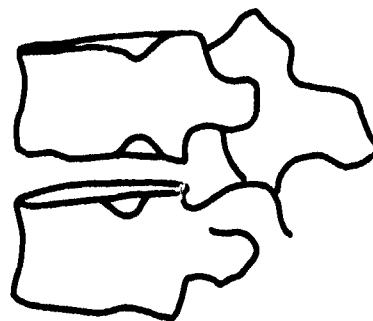
Radiologically concealed fractures consist of Schmorl's nodes and neural arch fractures. Schmorl's nodes, which are shown in Fig. 2, involve the herniation of nuclear material through the cartilaginous end plate. They involve end plate fractures but are seldom diagnosed because they are difficult to detect radiologically, Kazarian (1975). Schmorl's nodes are apparently due to compressive axial loads, which result in a state of hydrostatic stress in the nucleus. This induces both tensile membrane stresses and bending stresses in the end plates. The former arise from the need to confine the hydrostatically stressed nucleus radially, the latter from direct contact with the nucleus. Thus compressive loads generate tensile stresses in the end plates which can result in fractures.

In order to elucidate the source of neural arch fractures, it is advantageous to bear in mind the two load path model for the spine proposed by Prasad and King (1974). In this conceptualization, compressive loads are transmitted through two load paths: one path through the intervertebral discs and vertebral bodies, the second through the articular facets and processes. Any transfer of load between the two load paths would take place through the neural arches. In a simulation model, the transfer of load between the two load paths is indicated by a large difference in the loads borne by the upper and lower facets.

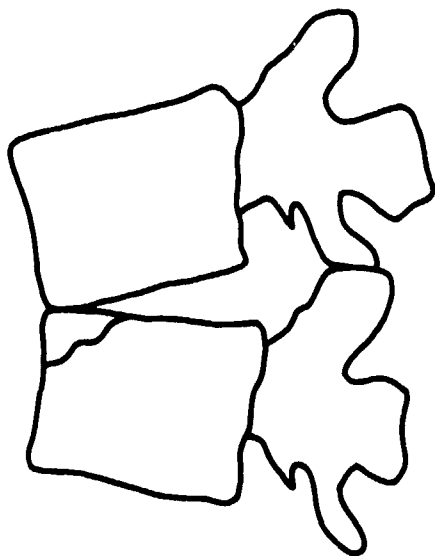
The last group of injuries, dislocations of the spine, are the most serious because they are often life threatening. The initiating factors for this type of injury are not as clear as the other groups of injuries. Some dislocations are characterized by complete compressive failure of the vertebral body and disruption of the facet joints. It is not clear whether the facet joint failure precedes the compressive vertebral body failure, or vice versa. If the latter is the sequence of events, then the possibility of dislocation failure can be related to extremely high compressive loads on the vertebral bodies.



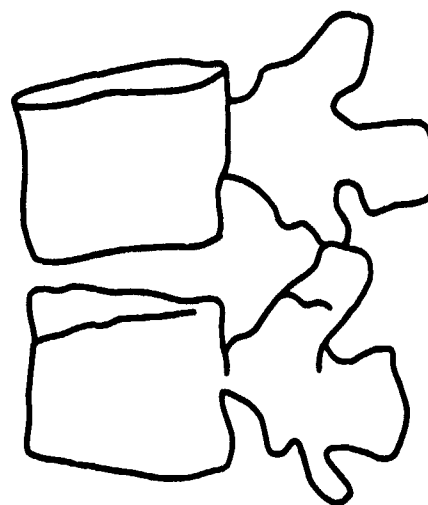
**COMPRESSION  
FRACTURE**



**SCHMORL'S  
NODE**



**ANTERIOR LIP (WEDGE)  
FRACTURE**



**MARGINAL RING  
(WEDGE TYPE) FRACTURE**

Figure 2. Vertebral body fracture patterns in  $G_z$  spinal impact from L.E. Kazarian et al (1968)

Some dislocations occur without compressive failure of the vertebral bodies, but solely as a result of facet joint disruption. Thus under large torsional loads, facet processes may fracture, followed by rupture of some of the posterior ligaments. This allows adjacent vertebrae to undergo large relative rotations about points considerably anterior to the spinal cord, resulting in the impingement of the bony posterior vertebral structures on the spinal cord or nerve roots.

Since spinal dislocations usually involve facet joint disruption, the magnitude and direction of the forces transmitted through this joint must be considered in the injury models. For dislocations caused by torsion or bending, criteria based on facet joint disruption may in fact prove sufficient. However, for dislocations accompanied by compressive vertebral body failures, the role of the facets cannot be considered exclusively.

Another failure mechanism which may be of importance under high load rates is hoop failure of the cylindrical part of the vertebral body. Kazarian and Kaleps (1979) report that such failures have been observed in animal experiments. A possible mechanism for this injury is the pressurization of the fluid which fills the voids in the trabecular bone. Under low rates of loading, this fluid can diffuse out of the vertebral body core through the end plates and the vascular system. However, under high load rates this is not possible, so the fluid within the core may behave in an incompressible manner and elevate the hoop stresses in the cortical shell of the vertebral body.

## SECTION III

### FINITE ELEMENT ANALYSIS

#### 3.1 Finite Element Model

A series of finite element models were developed for the first lumbar vertebra (L1) to determine the stress distributions and likely failure modes for static and rapid load rates, and to assess the accuracy of Belytschko's idealized model, which is illustrated in Fig. 3. The models assume small deformations and linear material behavior. Several load cases were studied; each employs a unit load. All of these load cases represent independent modes of deformation which through superposition can provide the stress distributions for more complex load combinations as will be illustrated subsequently.

Our first finite element models omitted the pedicles as shown in Fig. 4. A later model described in Section 4.4 includes the pedicles. The vertebral body model employed horizontal plane symmetry. As can be seen from Fig. 3, the taper in the x-z plane eliminates symmetry about the y-z plane. The cross section is an ellipse with the major axis coincident with the y-axis, the minor axis coincident with the x-axis. Although the model is symmetric about the sagittal plane (x-z plane), this symmetry could only be used for some of the loads, so it was not exploited here.

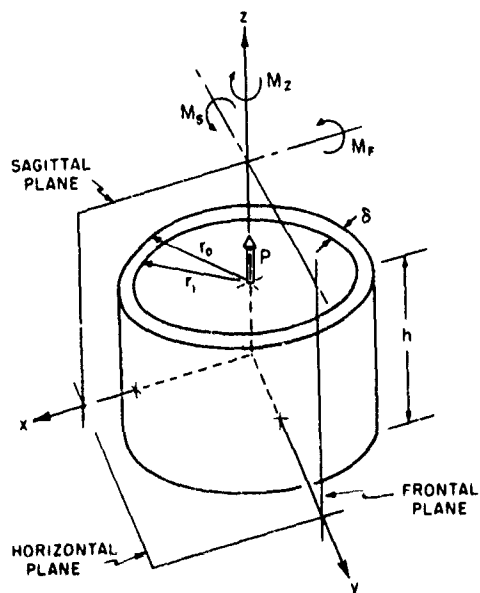
In addition to the perspective view, Fig. 4 gives a projection of the model into the x-z and x-y planes. As can be seen by a comparison of Figs. 3 and 4, the curved edges of the vertebra had to be approximated by piecewise linear surfaces. The trabecular core of the model is represented by 144 eight node isoparametric brick elements; 108 quadrilateral thin shell elements are used to represent the cortical bone surrounding the exterior. Only the exterior elements are shown in Fig. 4. The solid elements, which represent the trabecular core, are not shown.

A uniform thickness of 0.012 in., as reported by Kulak et al (1974), was assumed for the cortical bone. Elastic moduli of cortical and trabecular bone were those given by Evans (1970),  $2.18 \times 10^6$  psi and  $1.07 \times 10^4$  psi respectively. Poisson's ratio for both materials was taken as 0.25 for the static load rate analyses. For rapid load rates, Poisson's ratio was increased to 0.49 for the trabecular bone, which corresponds to a nearly incompressible material.

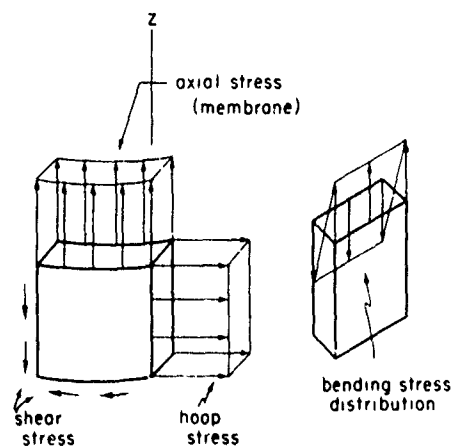
Two additional models of the vertebral body were developed to more closely model the true geometry of the human vertebra. The first refined model (Model 2) includes the variation of the cortical bone thickness in the end plates. In Model 3, the pedicles were added.



(a) idealized vertebral model  
with dimensions



(b) stress nomenclature



$$r_o = 0.799 \text{ in.} \quad r_i = 0.787 \text{ in.}$$

$$\delta = 0.012 \text{ in.} \quad h = 1.04 \text{ in.}$$

$M_F$  = Moment for bending in frontal plane

$M_S$  = Moment for bending in sagittal plane

$M_z$  = Moment for axial torsion

(c) sagittal and horizontal plane views of the first lumbar vertebrae  
(L1) with dimensions

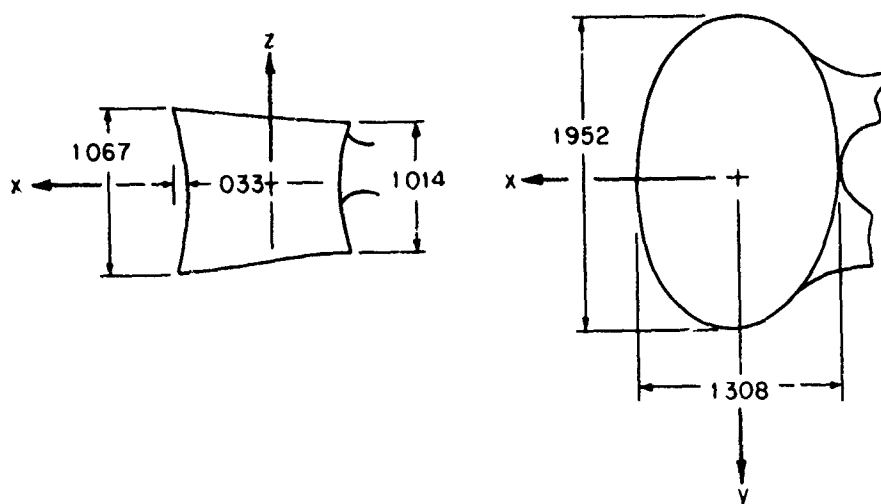


Figure 3. Vertebral models and stress nomenclature.

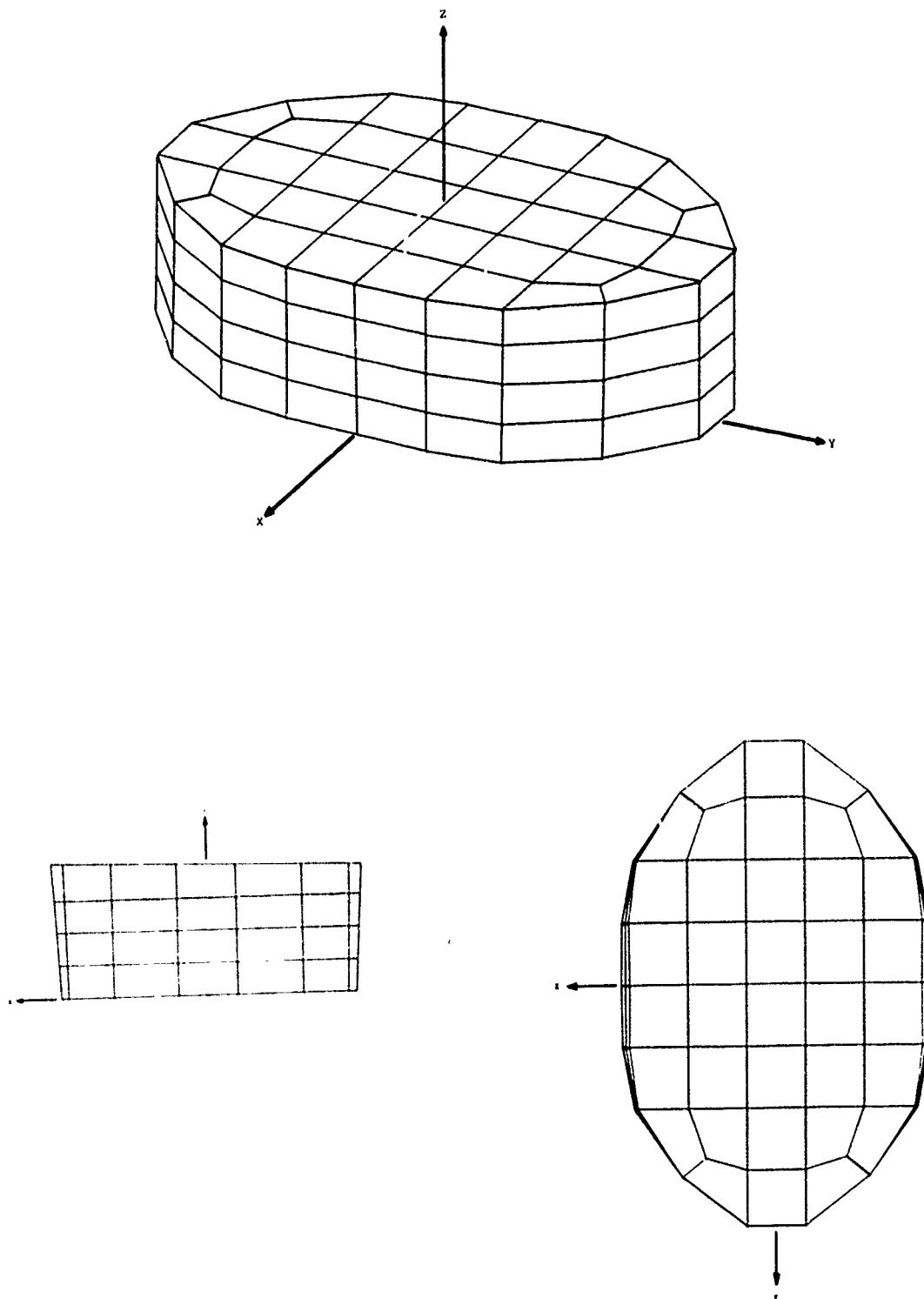


Figure 4. Finite element idealization of a vertebral body; perspective, sagittal plane and horizontal plane views. Dimensions for the first lumbar vertebra illustrated in Fig. 3c are used.

The stresses of interest are illustrated in Fig. 3. The stress in the vertical direction on a vertical face is called an axial stress; this is the stress which results directly from body weight. The stress in the circumferential direction on a circumferential face is called a hoop stress. Tensile hoop stresses are caused by internal pressurization of the vertebral body. The shear stresses are also shown. In the cortical bone, two types of stress distributions are considered: membrane states of stress, in which the stress is constant through the thickness, and bending states of stress, in which the stress varies linearly through the thickness, with equal absolute values but opposite signs on the inside and outside edges of the cortical bone. Each of the stress components has both a membrane and bending stress distribution. The total stress is always the sum of the membrane and bending distributions.

A general purpose finite element program, SAP, Wilson (1971), was employed for the analysis. Only static analyses were performed. The justification for the omission of dynamic effects is that during pilot ejection, the spinal column rarely experiences frequencies greater than 25 Hertz; higher frequencies are usually damped by the buttocks and soft tissue. The estimated fundamental natural frequency of a vertebra is greater than 6000 Hertz. Thus any dynamic response of the vertebra is unlikely. Details of frequency estimation are given in the Appendix.

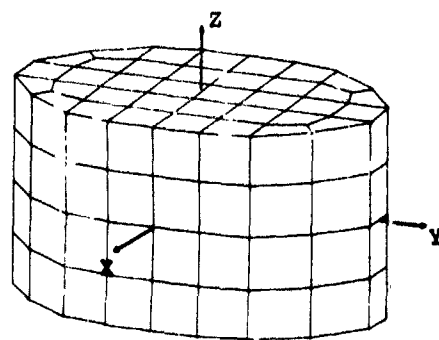
### 3.2 Axial Compression

A compressive axial load of 2.043 lbs. was uniformly distributed over the superior end plate of Model 1, which has an area of 2.043 in<sup>2</sup>, so that the average pressure was 1 psi. Both a compressible and an incompressible centrum were considered.

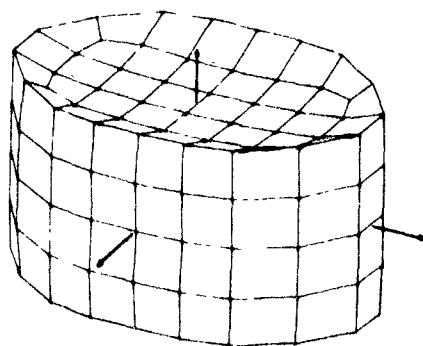
3.2.1 Compressible Vertebral Centrum. Deflections around the edges of the end plate were found to be minimal with deflections near the center of the end plate about one order of magnitude greater. This was due to the softness of the compressible trabecular core, as compared to the surrounding cortical shell. The deformations are shown in Fig. 5. These figures were obtained by magnifying the displacements, since the actual displacements would be invisible. This magnification leads to some misleading impressions: for example, since the undeformed vertebra tapers in at the x-axis, under axial compression it appears as if the point near the x-axis moves in. However, this is only due to the relative magnitudes of the taper and the magnified deflections.

The axial force causes concave bending of the end plate and convex bending of the sides. Fig. 5a illustrates an undeformed vertebra for the purpose of comparison.

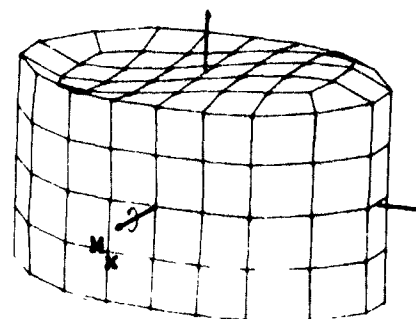
Stresses will be given in normalized units,  $P/A$ , where  $P$  is the axial force,  $A$  the end plate area. The cortical bone stress given by



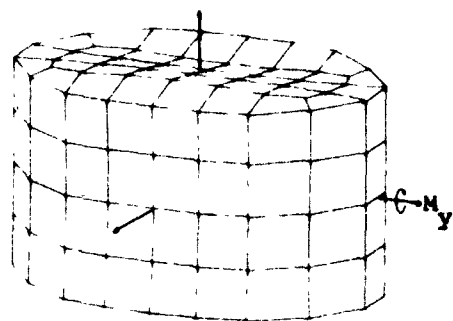
(a) undeformed vertebra



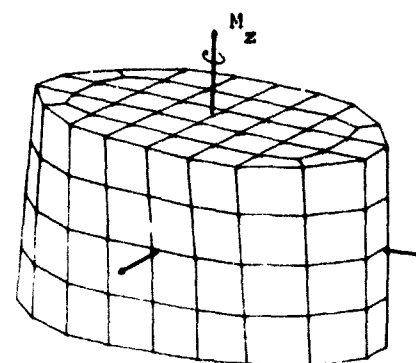
(b) deformation due to axial compression



(c) deformation due to frontal plane bending



(d) deformation due to sagittal plane bending



(e) deformation due to applied torque

Figure 5. Deformed shapes of a vertebra subjected to various loads.

Belytschko et al (1976) using the simplified model is

$$\sigma = \frac{E_o P}{\pi[E_i r_i^2 + E_o(r_o^2 - r_i^2)]} \quad (3.1)$$

where  $E_i$  and  $E_o$  are the Young's moduli for the trabecular (inner) and cortical (outer) bone, respectively, and  $r_i$  and  $r_o$  are the radii as shown in Fig. 3. For  $P = 2.043$  lbs., Eq.(3.1) yields a maximum stress of 28.9 psi or 28.9 P/A.

The membrane stresses in the cortical bone computed by the finite element model range from 7 P/A near the end plate to 14 P/A near the midplane. These stresses are perpendicular to the axial direction. The variation from top to center is caused by the redistribution of stresses from the trabecular to the cortical bone. Near the end plates, a larger portion of the load is carried by the trabecular bone. Towards the midplane of the vertebral body, some of this load is transferred to the more rigid cortical bone, so the stresses in the cortical bone increase while the stresses in the trabecular bone decrease. Fig. 6 illustrates the change in principal stress direction on a cross section of the vertebral body. Hoop stresses gradually increased from 4 P/A near the end plate to a maximum of about 13 P/A near the center of the side. Membrane stresses in the cortical bone on the end plate were small (<5 P/A).

Stresses due to bending were larger than the membrane stresses almost throughout the cortical bone. In the end plate, bending stresses were in the range of 9 P/A to 30 P/A. In the cylindrical part of the cortical bone, bending stresses are in the range of 9 P/A to 40 P/A. See Figs. 7 and 8 for profile of membrane and bending stress.

The highest stresses are in the anterior portion of the vertebral body near the end plates. This stress distribution is indicative of failure modes such as wedge fractures, which would probably initiate in the region adjacent to the anterior portion of the superior and inferior end plates.

3.2.2 Incompressible Vertebral Centrum. As stated earlier, the vertebral core response is incompressible when the load is applied very rapidly because of the hydrostatic pressure which is generated. In order to model this, Poisson's ratio was increased to 0.49 for the trabecular bone. All other parameters are unchanged.

With an incompressible centrum, the deflections of the end plate were reduced by 40%. Deflections across the end plate were almost constant except at the edges, where the curvatures are large.

The incompressibility increases the axial stiffness of the trabecular bone, and hence it carries a larger portion of the applied

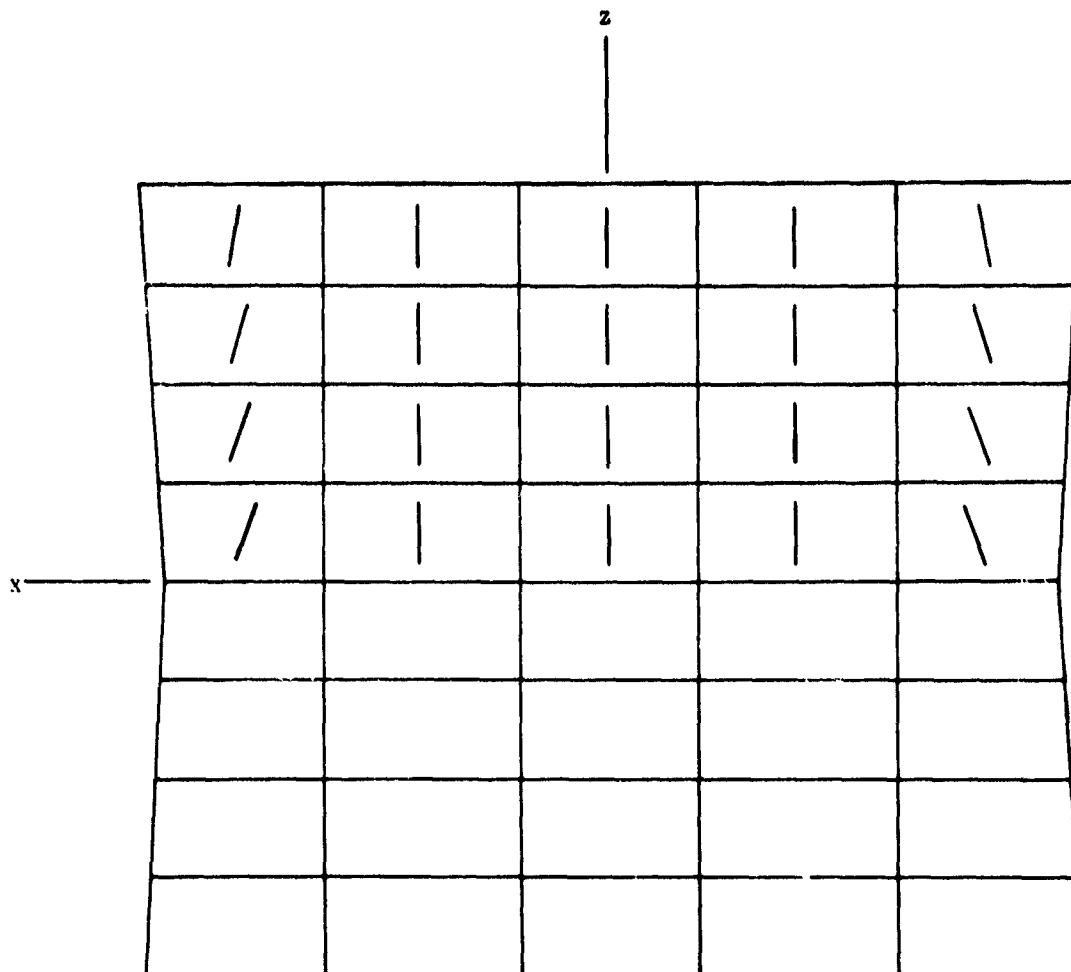


Figure 6. Trabecular bone principal stress direction for axial compression.

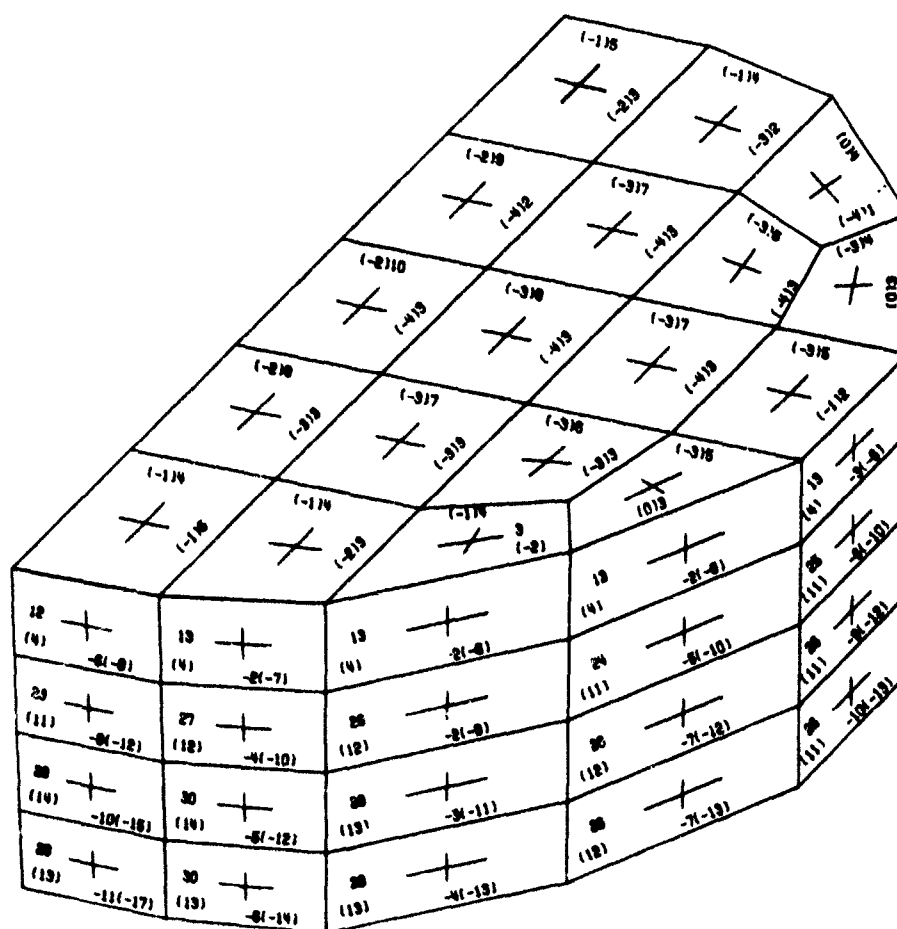


Figure 9. Cortical bone membrane stress distribution for axial compression with an incompressible centrum. Numbers in parenthesis are the corresponding stresses from the compressible centrum analysis. Stresses are in units of psi. Positive and negative values indicate tension and compression, respectively.

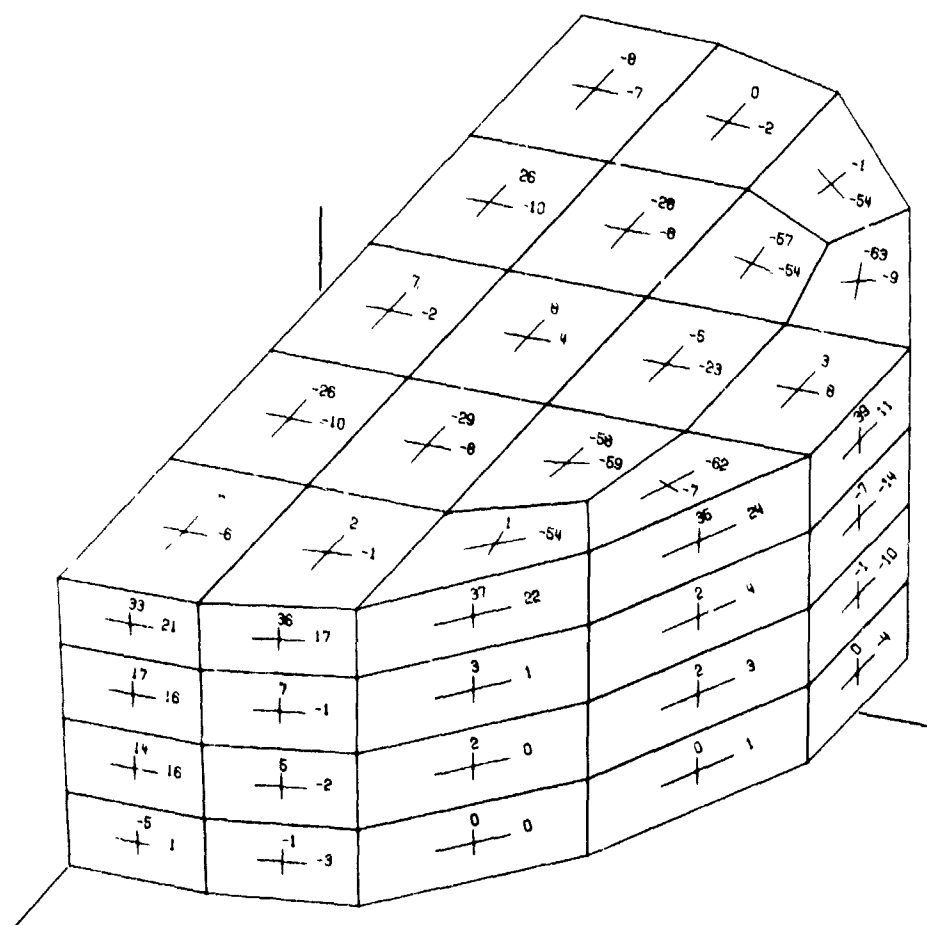


Figure 8. Cortical bone bending stress distribution for axial load. Stresses are in units of psi. Positive and negative values indicate tension and compression respectively on the exterior surface of the elements.



load. In the compressible analysis, the cortical and trabecular bone transmitted 42% and 58% of the axial load, respectively. For the incompressible core, 78% of the load is carried by the centrum. This has the effect of increasing trabecular bone stresses and decreasing cortical bone stresses.

The most significant change in the stress distribution was the increase in hoop stresses. Fig. 9 illustrates the membrane stresses for this analysis. Numbers in parentheses are the corresponding stresses from the compressible analysis. These stresses are twice that for the compressible core. In fact, the hoop stresses for the incompressible core are larger than the axial stresses, so that the mode of failure would probably be a bursting type, as opposed to the wedge fractures which are indicated by an analysis with a compressible core. Failures of a bursting type have been observed during animal impact experiments.

3.2.3 Comparison with Idealized Vertebral Model. The axial stress predicted by Eq. (3.1) is about  $29 P/A$ , which is two times greater than the maximum normal stress predicted by finite element analysis for the compressible core model. This discrepancy is due to the assumption in Eq. (3.1) that the strain in the trabecular core is the same as the strain in the cortical shell (i.e., that the end plate does not deform to a concave surface but remains flat). In the finite element model the strains in the trabecular bone, especially near the center are considerably greater than those in the cortical bone shell. This will tend to increase stresses in the trabecular core while proportionally decreasing stresses in the cortical shell. This can be clarified by considering the load distribution between the trabecular and cortical bone. Equation (3.1) predicts that the cortical and trabecular bone carry 86% and 14% of the applied load, respectively. The finite element analysis predicts 42% and 58%, respectively. It is this difference which causes Eq. (3.1) to predict much higher stresses for the cortical bone. However, stresses due to local bending of the cortical shell are neglected in Eq. (3.1). These bending stresses are quite large, and when combined with the membrane stresses yield values comparable to Eq. (3.1). It is not clear yet whether these large bending stresses are realistic. In any case, the membrane stresses given by the simplified model are substantially above that predicted by the more refined finite element computation.

### 3.3 Response to Bending Moments

Up to this point, only axial loads have been considered. However, an important consideration in the analysis of a vertebra is its response to various moments. Three moments will be considered: (1) a bending moment in the frontal plane; (2) a bending moment in the sagittal plane; (3) torsion, a moment about the z-axis (see Fig. 3). For the first two cases, the moment is generated by applying a linearly varying pressure on the end plate so that the axial force is zero. The magnitude of the pressure is chosen so that the applied moment is 1 in-lb.

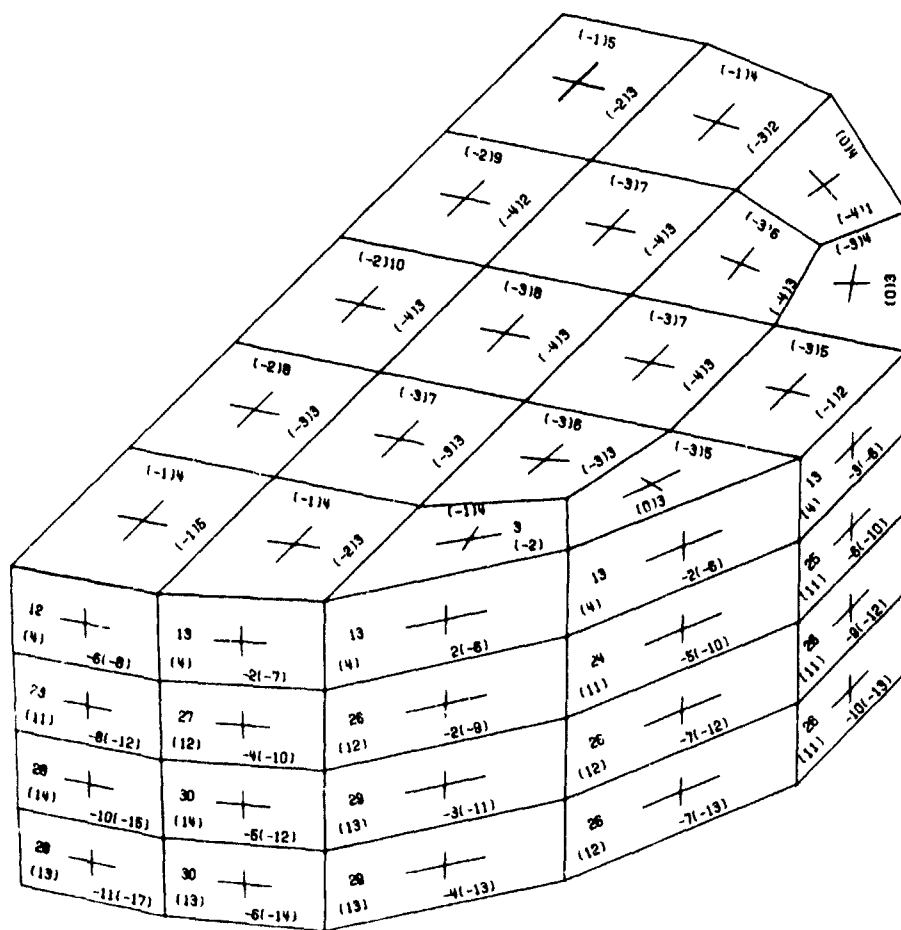


Figure 9. Cortical bone membrane stress d.tribution for axial compression with an incompressible centrum. Numbers in parenthesis are the corresponding stresses from the compressible centrum analysis. Stresses are in units of psi. Positive and negative values indicate tension and compression, respectively.

The pressure  $p$  for frontal plane bending, for example, is obtained from

$$p = Cy \quad (3.2)$$

where  $C$  is a constant and  $y$ , the distance from the  $x$  axis. The constant  $C$  is adjusted so that

$$\int_A Cy^2 dA = 1 \quad (3.3)$$

where  $A$  is the end plate area. The torque is generated by applying nodal loads in the plane of the end plate normal to the radial direction. Equations similar to Eqs. (3.2) and (3.3) were used to generate the nodal loads. A compressible vertebral core was used for all of the following analyses, except where noted otherwise.

3.3.1 Frontal Plane Moment. The deflections due to bending are shown in Fig. 5c. Part of the end plate is pushed up, part of it down, but near the cortical bone at the periphery the deflections were quite small. The deflection of the cortical shell on top was accompanied by bending of the sides as shown in the figure.

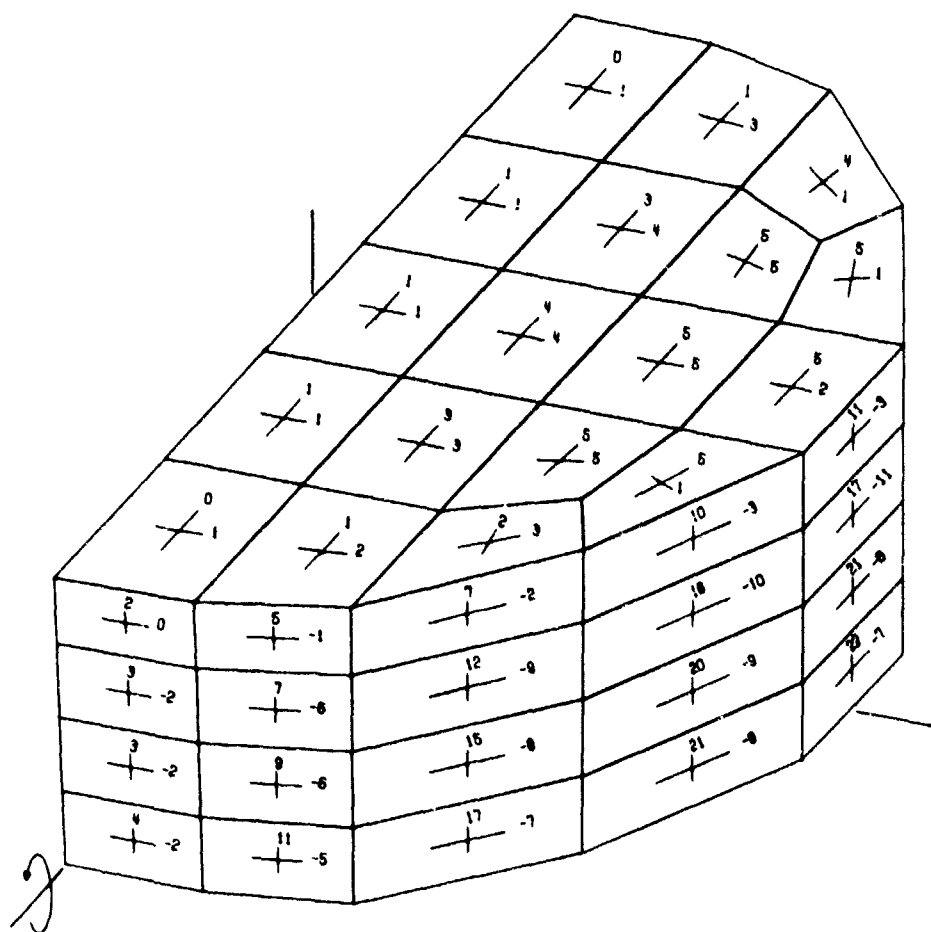
The stresses will be reported in terms of the stress given by the simplified model of Belytschko et al (1976),

$$\sigma = \frac{4ME_o r_o}{\pi[E_i r_i^4 + E_o(r_o^4 - r_i^4)]} \quad (3.4)$$

where  $M$  is the moment. Since this simplified model is circular, the stress predicted for frontal plane bending is the same as that for sagittal plane bending.

Membrane stresses in the cortical bone varied from a minimum near the  $x$  axis to a maximum of  $0.5 \sigma$  at the lateral edges. In all cases, the maximum stresses were axial stresses. Stresses due to local bending of the cortical shell were found to be considerably greater than membrane stresses. Membrane stresses in the end plate were negligible. Stresses as large as  $1.5 \sigma$  occurred in some parts of the end plates and lateral regions where the local bending of the shell was especially severe. Figures 10 and 11 show the membrane and bending cortical bone stresses for the applied moment. Since the extreme lateral regions of the vertebral body experienced the highest stresses, the mode of failure due to frontal plane moments would be a lateral wedge fracture.

3.3.2 Sagittal Plane Moment. The deformations due to sagittal



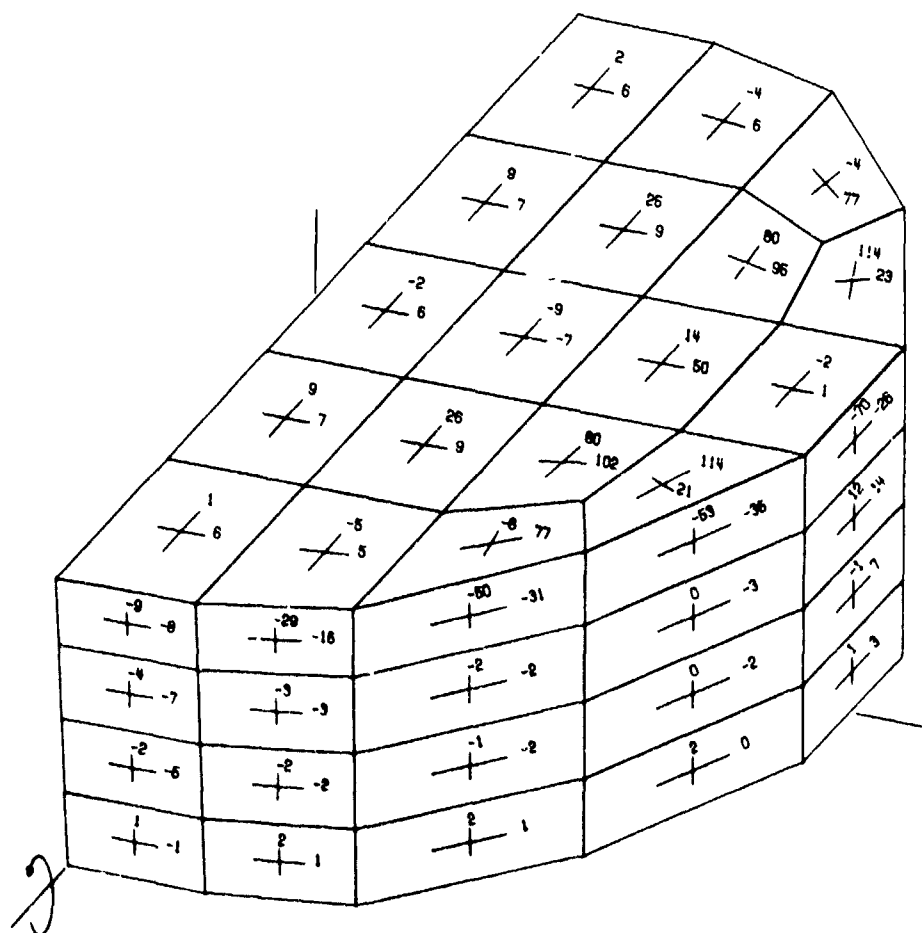


Figure 11. Cortical bone bending stress distribution for frontal plane bending. Stresses are in units of psi. Positive and negative values indicate tension and compression respectively on the exterior surface of the elements.

plane moments are shown in Fig. 5d. The general mode of deformation for sagittal plane moments is the same as for frontal plane moments. The maximum stresses are axial stresses. Due to geometry however, the vertebral body is less resistant to bending in this plane, so the membrane stresses are about 20% to 40% greater than for frontal plane bending. The bending stresses are only slightly higher. The most highly stressed area is the frontal region near the end plates, although high bending stresses also occur around the entire circumference of end plates. Due to the fairly high cortical bone stresses, shown in Figs. 12 and 13, wedge type fractures are highly probable in the entire frontal region.

Stresses predicted by Eq. (3.4) are roughly two times greater than the maximum stresses in the finite element analysis. The source of the discrepancy is the assumption that plane sections remain plane, which was used in deriving Eq. (3.4). The finite element results do not conform to this assumption. As stated earlier, the deflections of the trabecular core are considerably greater than that of the cortical shell. This causes warping of the cross section, which in turn leads to a strain distribution which increases trabecular stresses and decreases cortical stresses. In addition, the warping causes severe localized bending of the cortical bone shell. These bending stresses vary substantially, but in many locations are two times greater than the stress predicted by Eq. (3.4).

We also considered the effect of vertebral centrum compressibility on the response to bending moments. Increasing Poisson's ratio to 0.49 for the trabecular bone (incompressible vertebral centrum) decreased the end plate deflection by approximately 20% and decreased axial membrane stresses in the cortical bone by about 10% to 20% for both frontal and sagittal plane bending. The stress distribution was not altered significantly except that the hoop stresses increased by 100% to 150%. As a result, the hoop stresses are of the same order of magnitude as the axial stresses in the cylindrical portion. Therefore, with an incompressible core, the failure mode for pure bending is not clearly delineated by the analysis. Failure in either a wedge mode or a bursting mode is possible.

3.3.3 Torsion. For the analysis of torsion, midplane symmetry could not be used, so a model of the entire vertebral body was used. This required 144 solid elements for the trabecular bone centrum and 144 shell elements for the cortical bone (36 additional shell elements were included to cover the inferior end plate). Half of this slightly coarser mesh is shown in Fig. 14.

The deformation due to torsion was a typical twisting motion with little local bending, as shown in Fig. 5c. For the sake of comparison, stresses will be reported in terms of the shear stress given by strength of materials theory for the simplified model

$$\tau = \frac{2M_z r_o}{\pi[r_o^4 - r_i^4]} \quad (3.5)$$

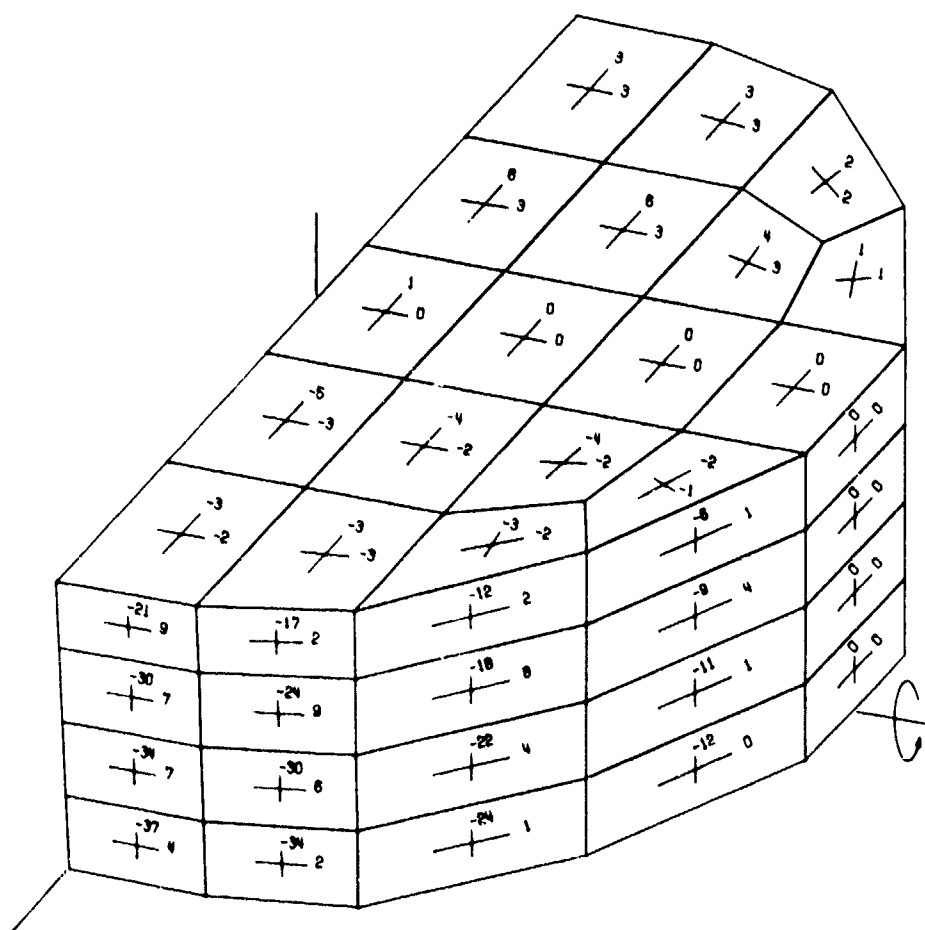


Figure 12. Cortical bone membrane stress distribution for sagittal plane bending. Stresses are in units of psi. Positive and negative values indicate tension and compression, respectively.

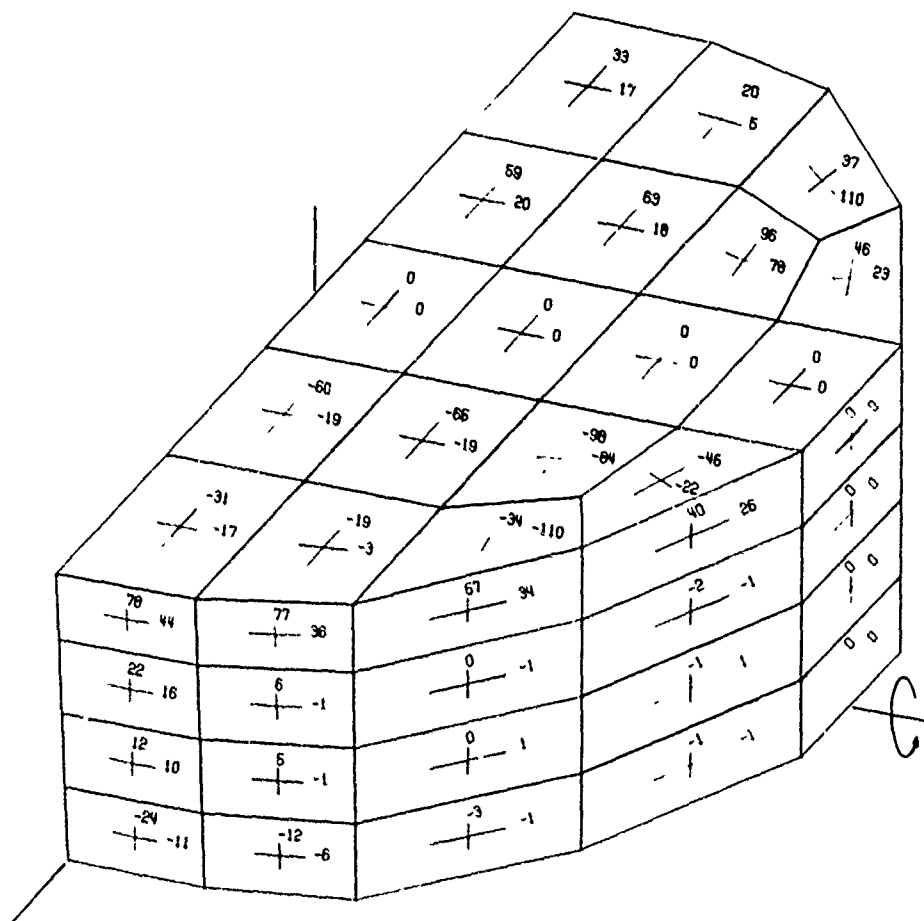


Figure 13. Cortical bone bending stress distribution for sagittal plane bending. Stresses are in units of psi. Positive and negative values indicate tension and compression respectively on the exterior surface of the elements.



where  $M_z$  is the applied torque. For a unit torque of 1 in-lbs, Eq. (3.5) yields a cortical bone shear stress of 21.3 psi.

Figure 14 shows a profile of shear stresses along the sides of the vertebral body. Membrane and bending stresses throughout the entire cortical bone shell were small. Shear stresses in the lateral region are almost uniformly  $0.95\tau$ . Shear stresses on the end plate were also uniform at  $0.5\tau$  to  $0.75\tau$ . From these results, it is apparent that Eq. (3.5) predicts the maximum cortical shear stresses quite well.

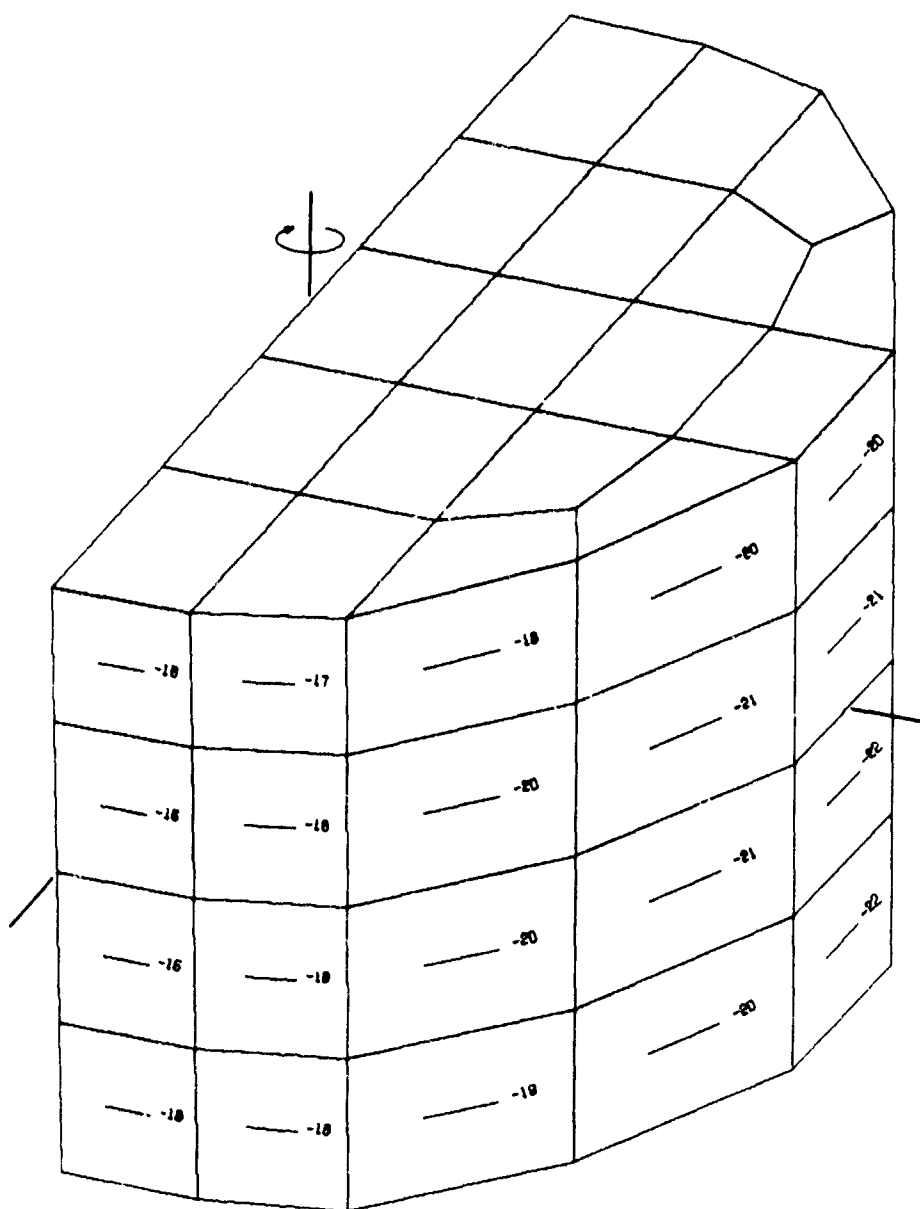


Figure 14. Cortical bone shear stress distribution for axial torsion. Stresses are in units of psi. Only half of the mesh is shown.

## SECTION IV

### REFINED FINITE ELEMENT MODELS

#### 4.1 Effects of Small Changes in Cortical Bone Thickness

A uniform cortical bone thickness of 0.012in. was assumed initially. In reality, the thickness may not be uniform and may differ from this value. Therefore an analysis under axial load with Model 1 was made using a constant shell thickness of 0.016 in. Despite this substantial increase in cortical bone thickness, deflections and stresses were decreased by only 10% to 20%. It appears that moderate changes in cortical bone thickness (20 to 30%) will have the same order effect on the resulting deflections and stresses.

#### 4.2 Finite Element Model 2 (Variable End Plate Thickness)

The thickness of cortical bone decreases at the center of the end plates. To model this, the end plate thickness was linearly tapered from a maximum of 0.012in. near the edge to a minimum of 0.0012in. at the center. This modification constitutes Model 2. The resulting deflections and stresses were virtually unchanged except for a 10 to 15% reduction in hoop and bending stresses in the lateral region immediately adjacent to the end plates.

#### 4.3 Finite Element Model 3 (Effects of Pedicle)

In the studies described so far, it was assumed that reasonable results can be obtained without considering the effects of the pedicles. To investigate this assumption, Model 2 was refined by adding 25 posterior 8 node isoparametric brick elements to represent trabecular bone and 52 quadrilateral thin shell elements to represent cortical bone as shown in Fig. 15. Only sagittal plane symmetry was used.

A detailed geometric representation of the posterior structure was not needed in these studies because only the load transfer from the facets to the vertebral body was of interest. Only the junction of pedicle and vertebral body, which is also the likely site of high stresses, was modeled in detail.

One 8 node solid element was used to represent the superior articular process in order to facilitate the application of facet loads. Several solid and shell elements were used to represent the lamina; these extended from the pedicle to the plane of symmetry to

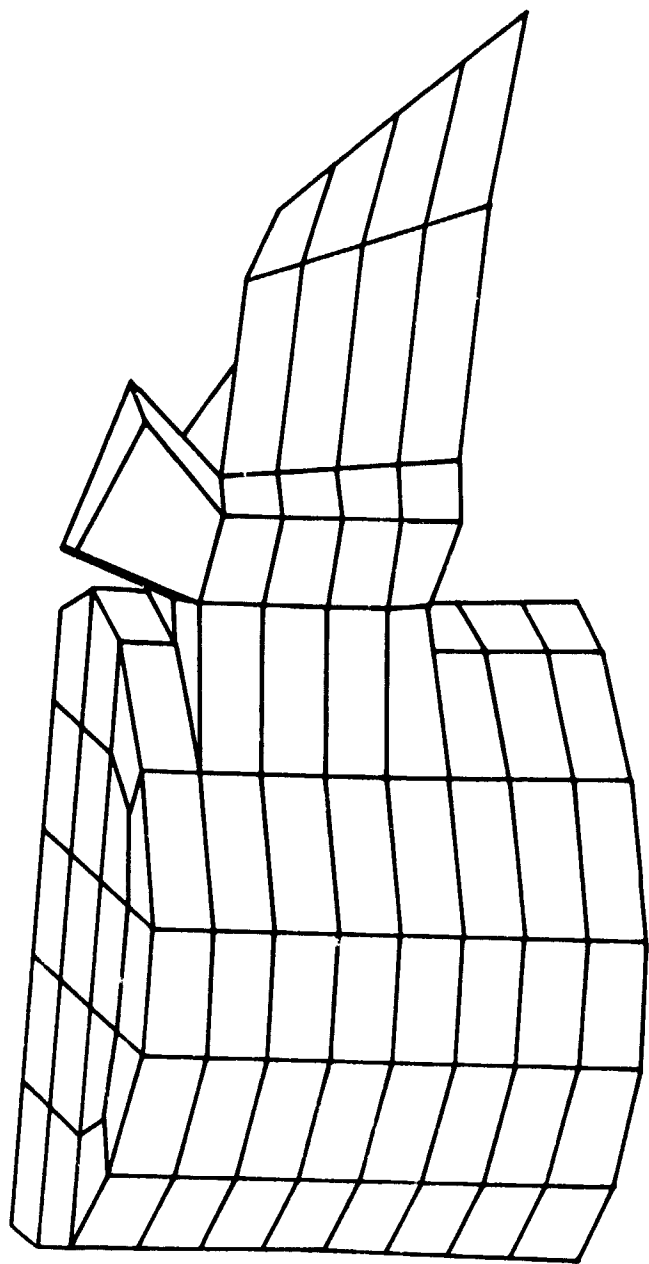


Figure 15. Finite element model of vertebral body including posterior structure. (Model 3).

account for the stiffness provided by the pedicle. Material properties and cortical bone thickness were the same as those in the previous analyses; (Model 2). The core of the vertebral body was assumed to be compressible.

Support conditions present a difficulty in this analysis. In the spinal column, compressive loads are transmitted through intervertebral discs, and in the center region the disc is almost in a hydrostatic state of stress. Thus, the load distribution on the center region of the end plates is relatively uniform. For this reason, supporting the vertebral body at a few selected points might lead to erroneous results, since the reaction forces would differ substantially from that in the motion segment.

Analyses for compressive axial loads reported in Section 3.1 indicated that the rim of the end plate does not distort very much, but simply translates. Thus, after application of the load, all points along the rim of the end plate lie approximately in the same plane. Assuming that this is unchanged with the addition of the pedicles, the rim of the inferior end plate was rigidly supported, preventing out of plane deflection.

Two load cases were considered: (1) a uniform axial load was applied simultaneously to the superior end plate and in the opposite direction on the inferior end plate; the load was equal in magnitude to that used in Section 3.1, 2.043 lbs. (2) a compressive load applied to the superior articular process; the total load was 1 lb., which was divided between two nodes which represent the facet.

4.3.1 Axial Compression. This analysis was designed to investigate the effect that the pedicles might have on the stress distribution.

The vertebral body was loaded over the end plates as before, and the results are compared to those obtained by a model which omits the pedicles. Membrane stresses on the sides and the end plates were unchanged, except for a 30 to 60% increase in stresses in the frontal region adjacent to the anterior of the superior end plate and a 50 to 75% increase in cortical bone stresses in the vertebral foramen. Bending stresses in the cortical bone generally remained the same or decreased somewhat. Stresses on the end plate showed a 10% increase. Figures 16 and 17 show frontal and posterior views of the membrane stress distributions. Figures 18 and 19 provide frontal and posterior views of the bending stress distributions. Numbers in parentheses are stresses obtained from the analysis without the pedicle, which were previously given in Figs. 7 and 8. For clarity, most of the posterior structure is not shown. As can be seen from these results, the presence of the pedicle has little effect on the stresses in the vertebral body caused by axial loads.

4.3.2 Facet Load. In the human vertebral column, a second load path is provided through the superior and inferior articular

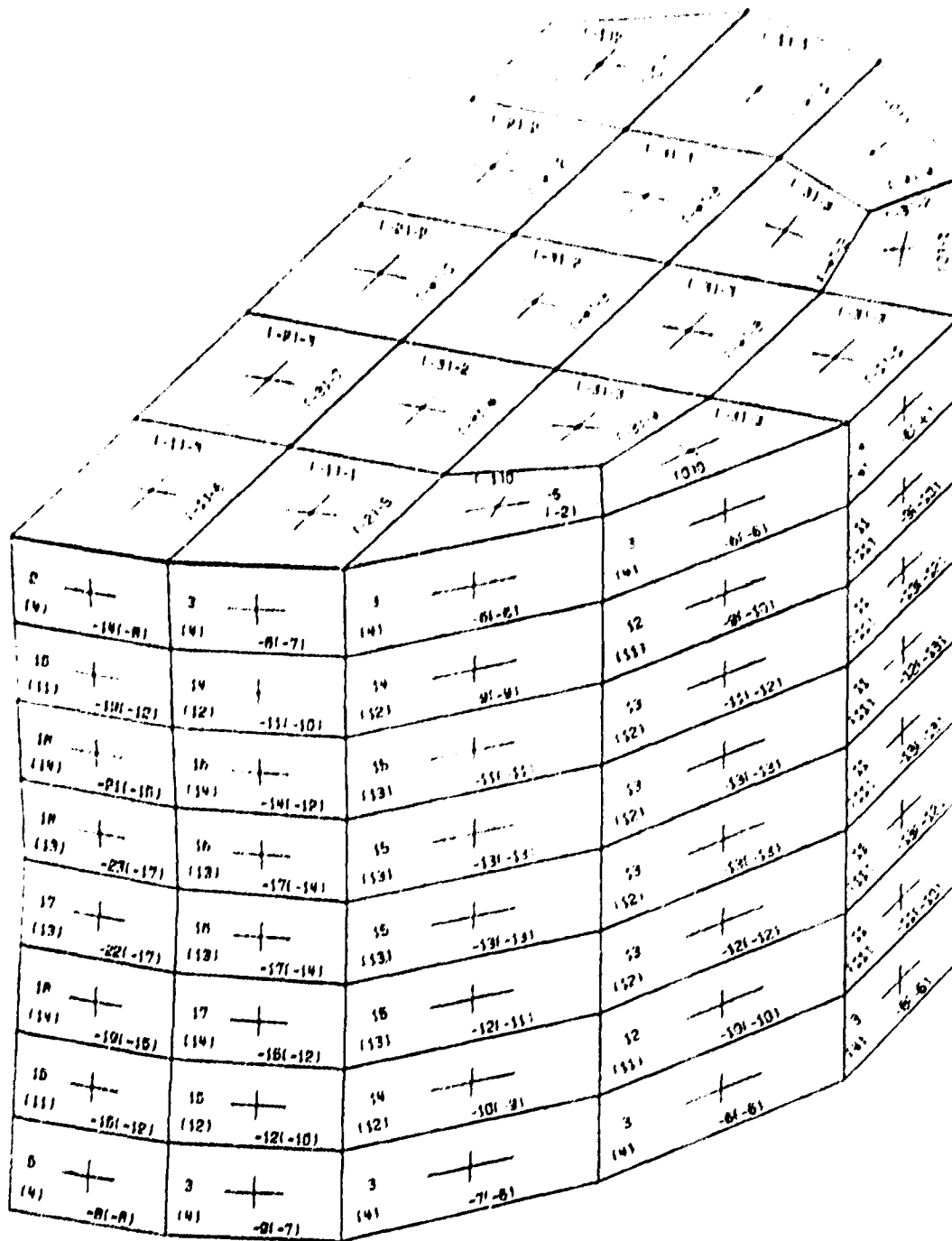


Figure 16. Frontal view of the cortical bone membrane stress distribution for axial compression. Numbers in parenthesis are the corresponding stresses from analysis neglecting effects of the pedicle. Stresses are in units of psi. Positive and negative values indicate tension and compression, respectively.

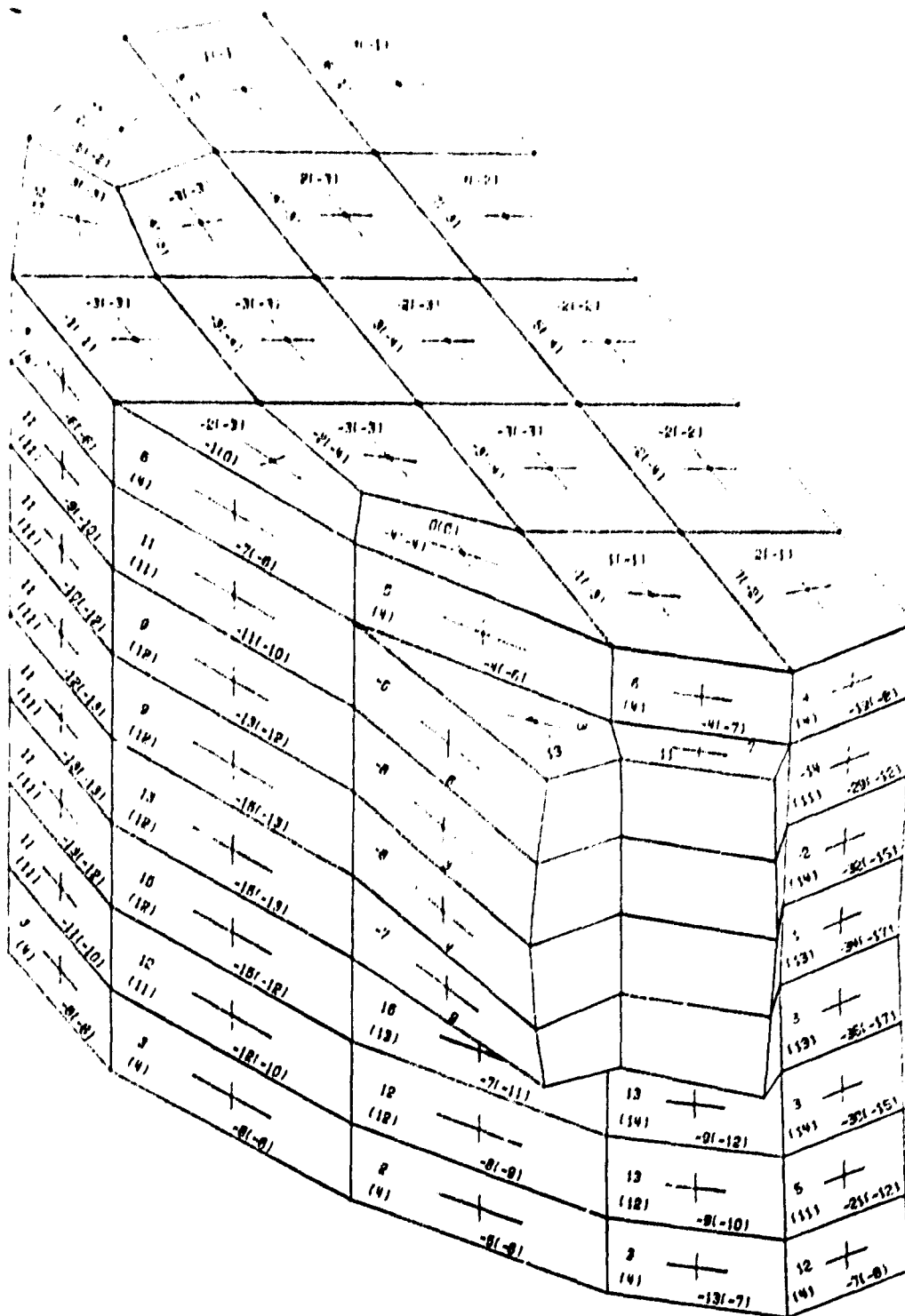


Figure 17. Posterior view of the cortical bone membrane stress distribution for axial compression. Numbers in parenthesis are the corresponding stresses from analysis neglecting effects of the pedicle. Stresses are in units of psi. Positive and negative values indicate tension and compression, respectively.

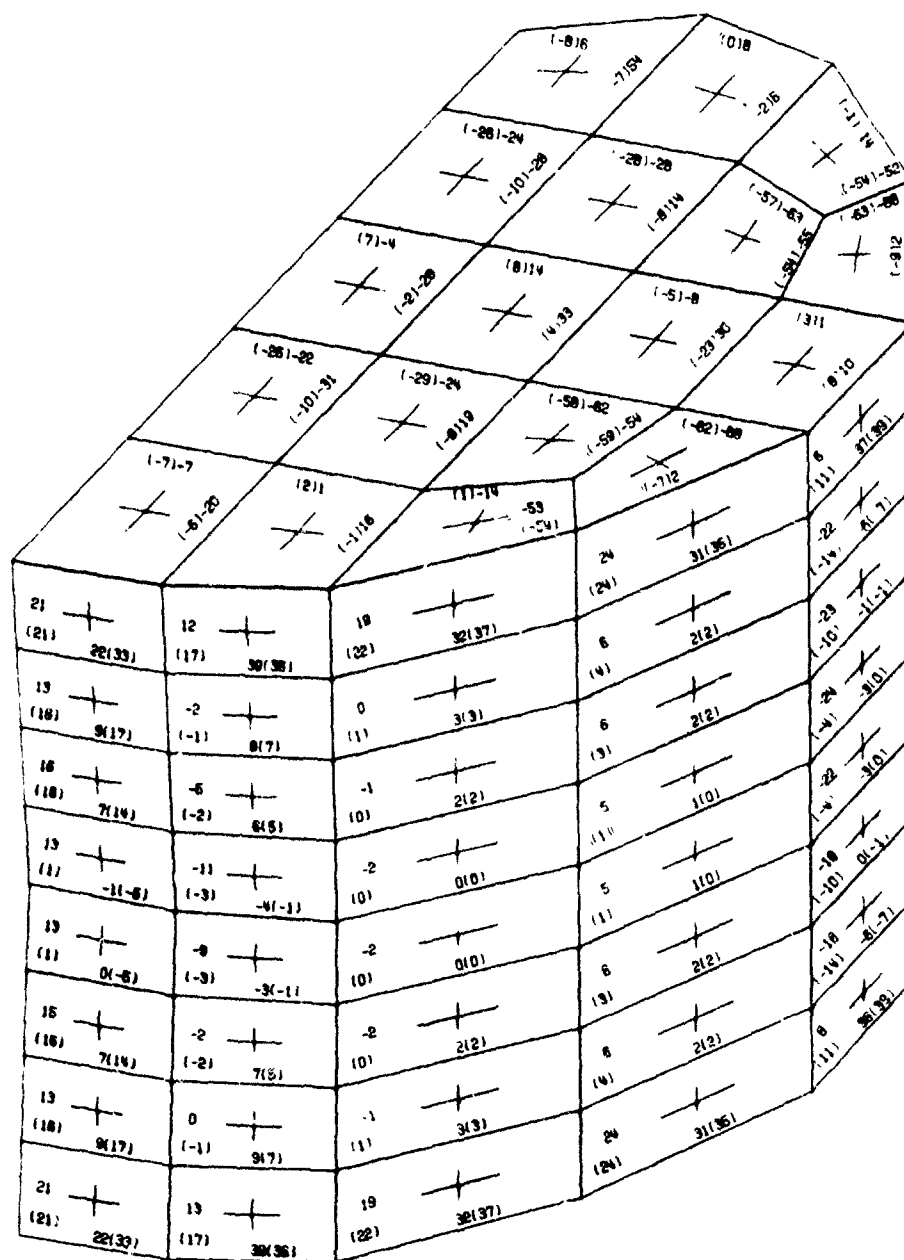


Figure 18. Frontal view of the cortical bone bending stress distribution for axial compression. Numbers in parenthesis are the corresponding stresses from analysis neglecting effects of the pedicle. Stresses are in units of psi. Positive and negative values indicate tension and compression respectively on the exterior surface of elements.



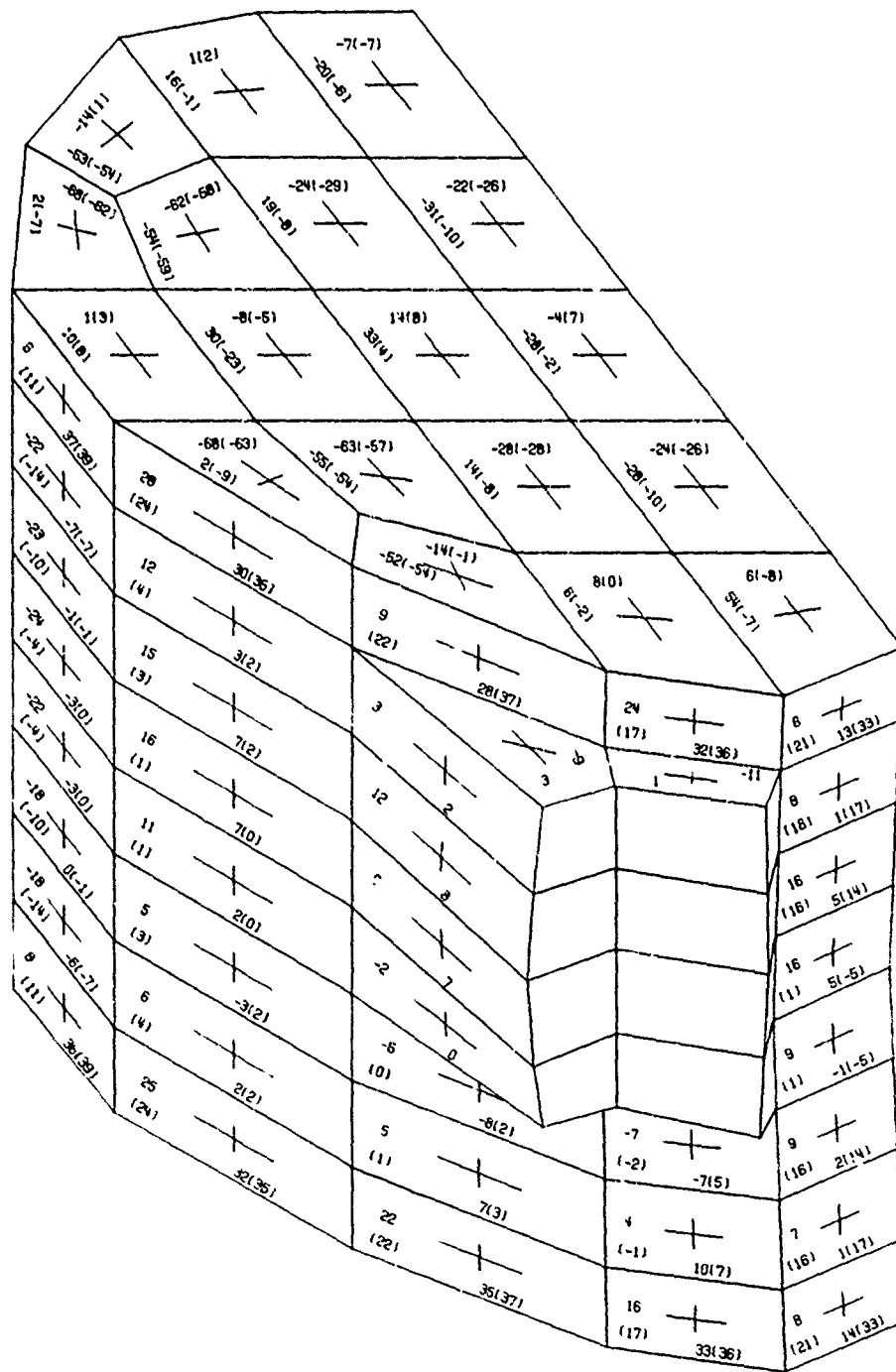


Figure 19. Posterior view of the cortical bone bending stress distribution for axial compression. Numbers in parenthesis are the corresponding stresses from analysis neglecting effects of the pedicle. Stresses are in units of psi. Positive and negative values indicate tension and compression respectively on exterior surfaces of elements.

processes. When the forces on the superior and inferior processes are not equal, the balance is transmitted through the pedicle to the vertebral body. This analysis considers the resulting stresses due to a compressive load on the superior articular process. The load was of unit magnitude and applied to two nodes. Since the analysis is linear, stresses for higher loads can be obtained simply by multiplication.

Axial membrane stresses in the frontal region ranged from 2 psi near the superior end plate to almost 50 psi near the inferior end plate. Stresses in the lateral region varied from 11 psi tension to 40 psi compression. Membrane stresses in the posterior region increased significantly near the junction of the pedicle. High compressive and tensile stresses occur throughout this region. The stresses are especially severe directly beneath the pedicle, where stresses are as high as 170 psi. Figure 20 and 21 illustrate frontal and posterior views of the resulting membrane stress distributions.

Comparison of the total loads transmitted through the cortical bone elements illustrated in Fig. 22 and the adjacent trabecular

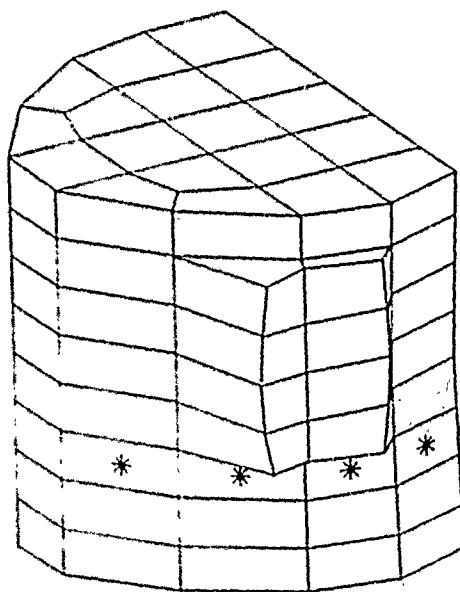


Figure 22. Illustration of the elements used in the analysis of facet load transfer.

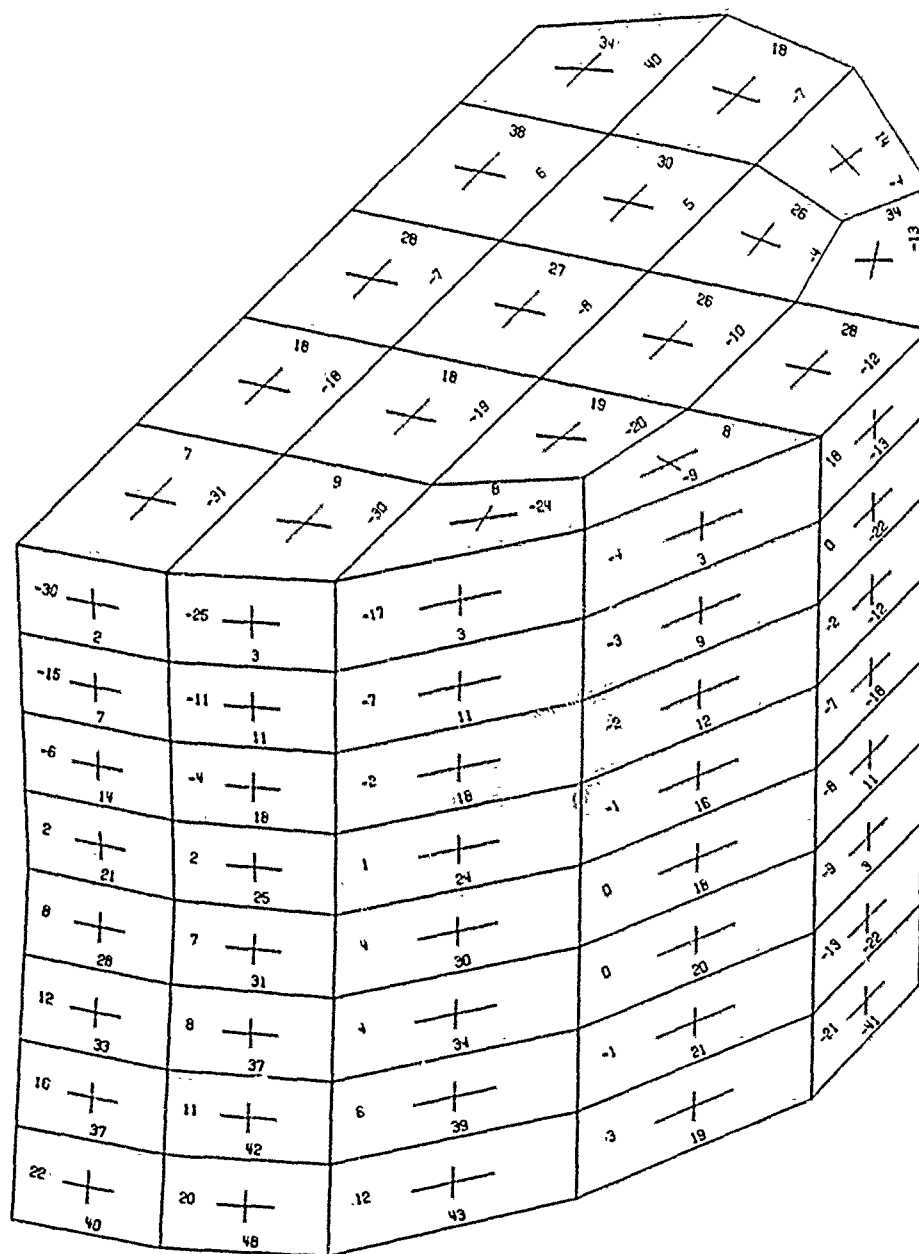


Figure 20. Frontal view of the cortical bone membrane stress distribution for facet loading. Stresses are in units of psi. Positive and negative values indicate tension and compression, respectively.

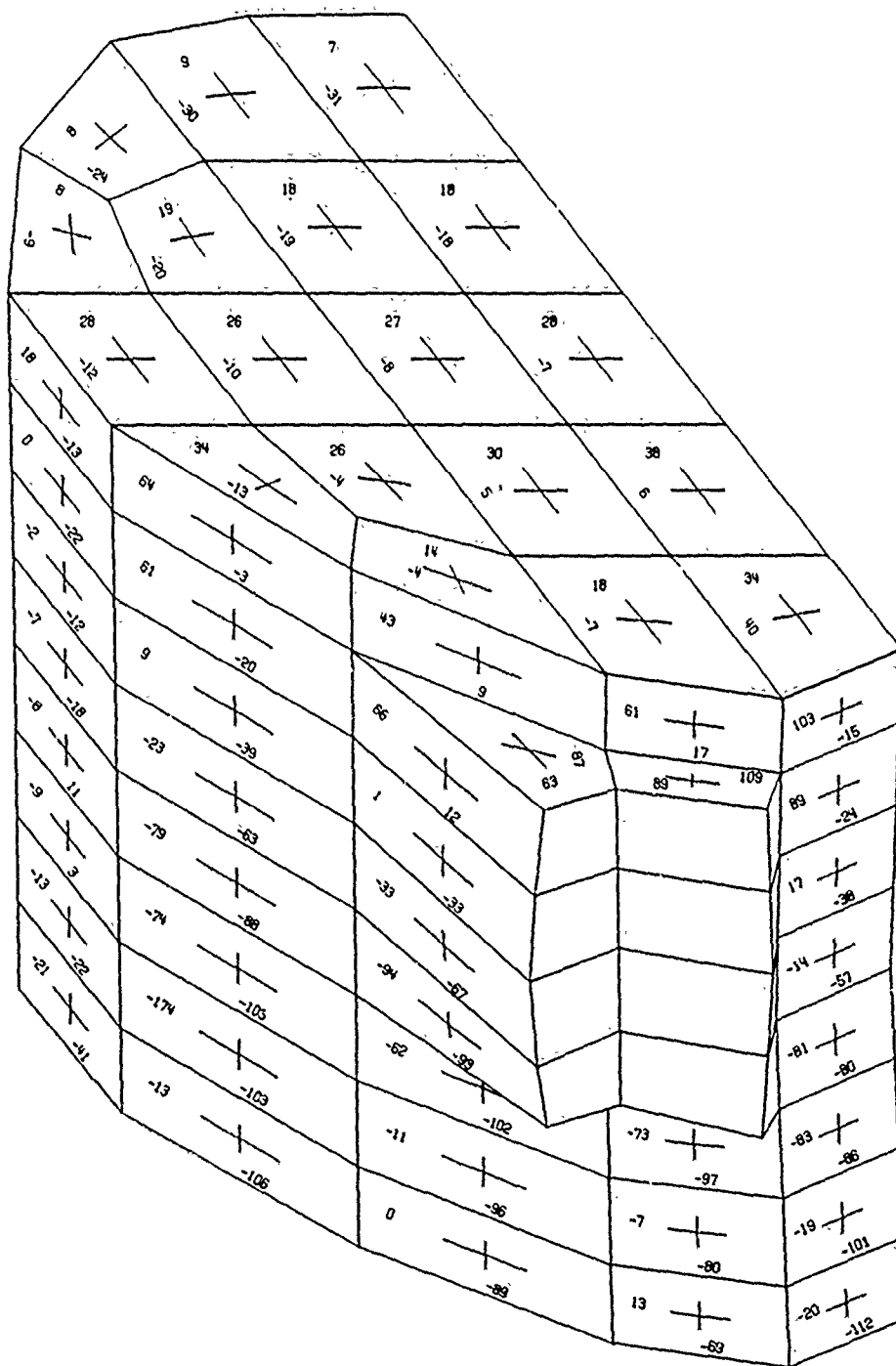


Figure 21. Posterior view of the cortical bone membrane stress distribution for facet loading. Stresses are in units of psi. Positive and negative values indicate tension and compression, respectively.

bone elements indicates that the cortical bone carries an order of magnitude more load than the trabecular bone. The large stresses in the cortical bone in this region may be caused by the support conditions, since only the rim of the inferior end plate is supported, allowing the rest of the end plate to deflect. However, even if a different support condition were used, the cortical bone would probably still carry more load than the trabecular bone because the cortical bone stiffness is several orders of magnitude greater than the trabecular bone stiffness. Since the strain gradient in this region is very small, the trabecular bone will not develop high stresses and hence the trabecular bone will carry little load. It should be noted that to verify this analysis and in particular, the small strain gradients, a more refined model would be needed. This was not feasible at this time. If the model is appropriate, then it indicates that the facet loads are transmitted from the pedicles to the inferior end plate primarily through the cortical bone.

Figure 23 and 24 illustrate frontal and posterior views of the bending stresses. Stresses due to bending of the cortical bone were small in the frontal region, gradually increased in the lateral region, and were maximum near the pedicle junctions. Stresses as high as 280 psi occurred on the vertebral body. Stresses around the circumference of the pedicle were as high as 500 psi. These high pedicle stresses would be reduced if the posterior cortical bone were thicker. Again, it is not clear whether these high stresses are due to sharp corners in the model or reflect reality. This could only be answered by the use of a more refined model.

The stresses under combined axial loading and pedicle loading can be obtained by superimposing stresses from the axial load analysis and the facet load analysis. For example, if stress results are desired for a load case involving 750 lb. distributed on the superior end plate, and 250 lb. applied on the superior articular process, then the resulting stress at any location can be obtained by multiplying the axial load stresses by 750 and adding them to 250 times the stress from the facet load analysis in the corresponding location. More complex load cases can be considered by using results of sagittal and frontal plane bending.

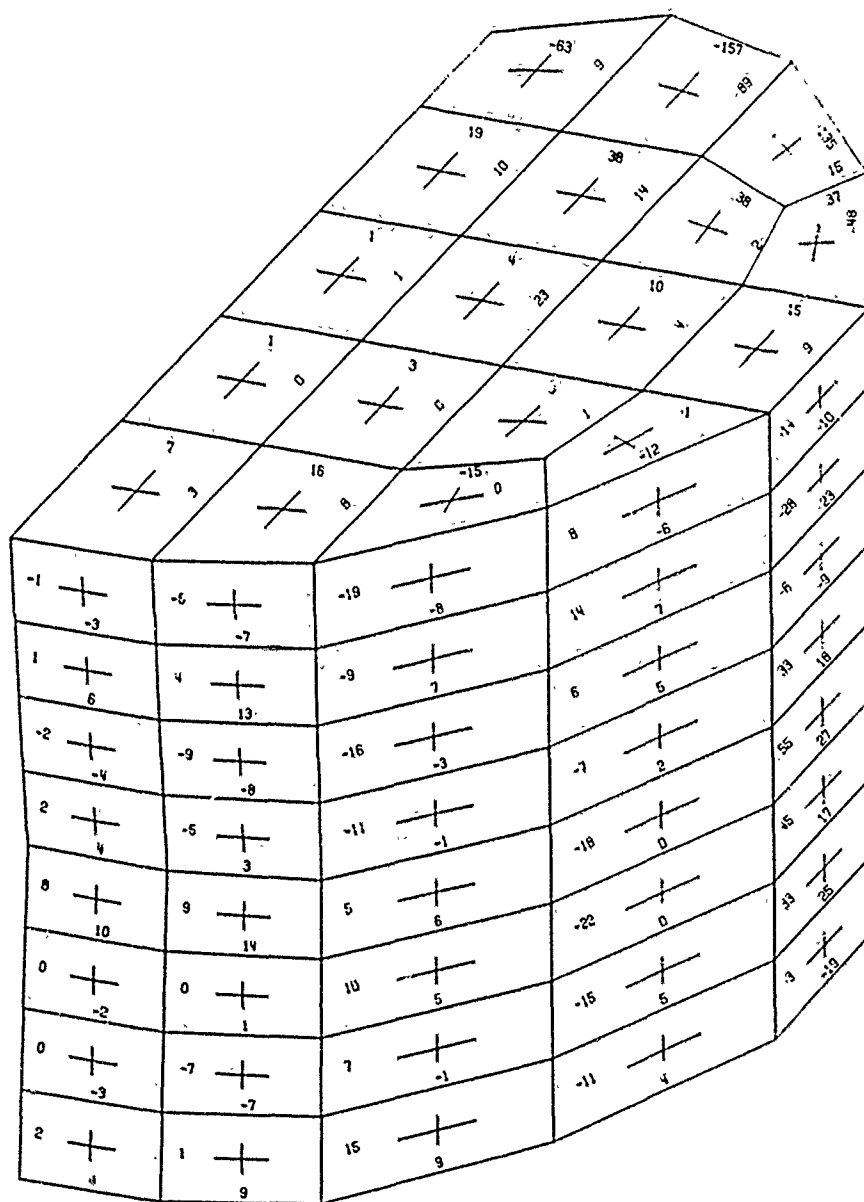


Figure 23. Frontal view of the cortical bone bending stress distribution for facet loading. Stresses are in units of psi. Positive and negative values indicate tension and compression respectively on the exterior surface of elements.

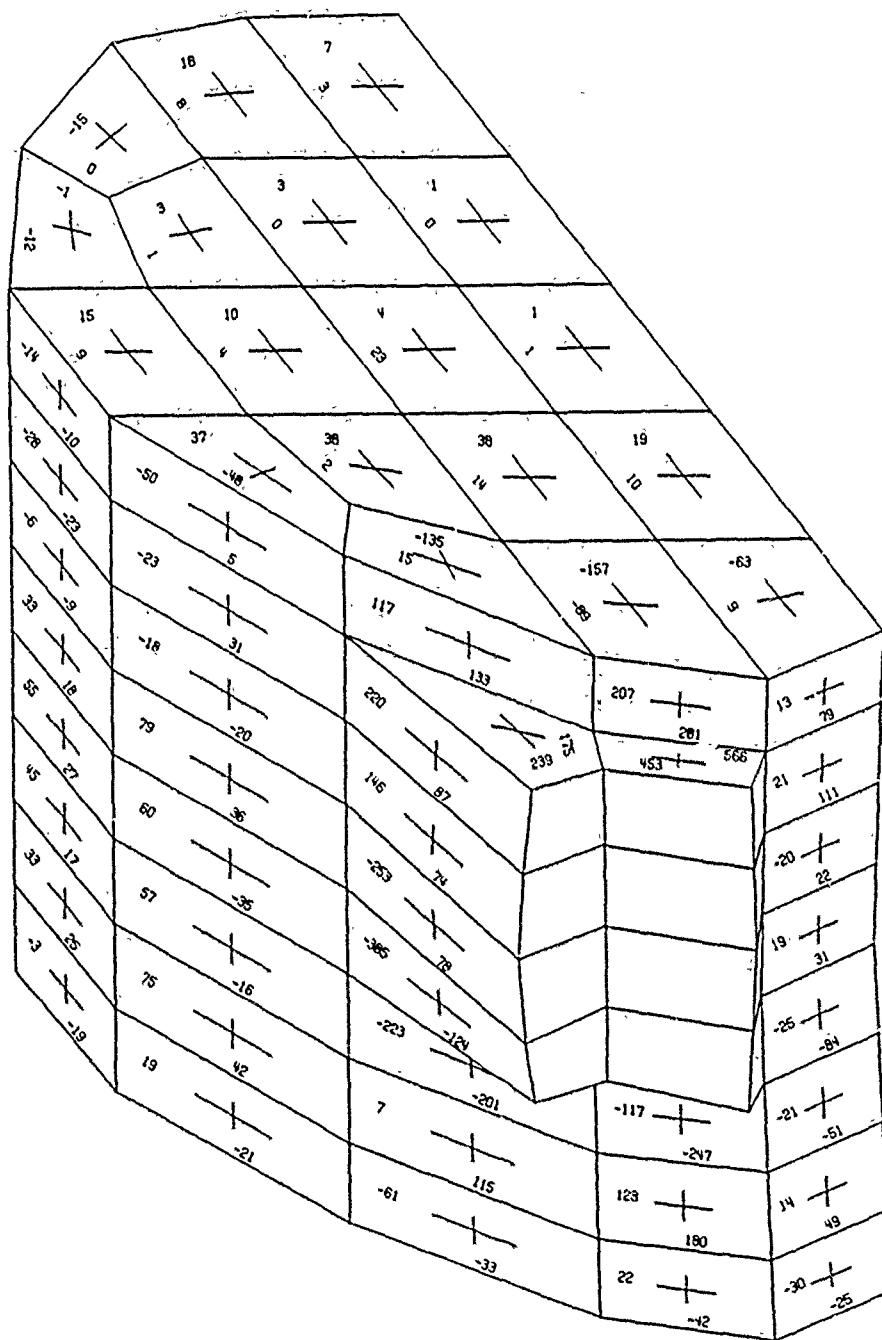


Figure 24. Posterior view of the cortical bone bending stress distribution for facet loading. Stresses are in units of psi. Positive and negative values indicate tension and compression respectively on the exterior surface of elements.

## SECTION V

### CONCLUSIONS

Finite element analyses of a lumbar vertebra have been performed to evaluate the effectiveness of a previously developed simplified model and to gain a better understanding of stress distributions due to axial load, frontal and sagittal moments, and torsion. The finite element analyses employed isotropic linear-elastic models. Both compressible and incompressible vertebral centrams were considered.

For the compressible centrum, the maximum stress under axial load is the axial stress, which is the only stress considered in the simplified model. However, the finite element model showed that the membrane stresses in the cortical bone are only about a third of those predicted by the simplified model. This discrepancy arises from the assumption of a state of uniform strain in the simplified model, which results in an underprediction of the load carried by the trabecular bone.

The finite element model also predicts substantial stresses due to bending moments in the cortical bone shell. These stresses have a linear distribution through the thickness of the cortical bone, so the maximum stress is the sum of the absolute values of the bending and membrane stresses. The validity of these large bending stresses is not clear; they may be an idiosyncrasy of the model rather than reflective of reality. In the model, the transition from trabecular to cortical bone is discontinuous both in material properties and element type, while the physiology of the vertebra has a smoother, more continuous transition. Furthermore, the high stresses predicted by the finite element model violate the prevalent theme of optimum design in biological structures. The validity of this model is under serious scrutiny; however, only by extreme mesh refinements can answers to these questions be achieved.

If only the membrane stresses predicted by the finite element models are valid, the simplified model may still be applicable provided that a reduction factor based on detailed studies such as this are used to account for the load transmission through the trabecular bone. The simplified model can only be valid if compressive failures are likely; since it neglects hoop stresses. The finite element analyses show large differences in the response of compressible and incompressible centrams. Compressive, or wedge type failures are predicted for compressible centrams, while bursting type failures are characteristic of incompressible centrams.

For torsional loads, the simplified model agrees quite closely



with the finite element model. Under bending moments, the agreement is not as good.

To study the effect of various anatomical features of the vertebra, several additional finite element models were developed. We observed that when posterior loads are unimportant, good accuracy could be obtained by considering a model which neglects the pedicles. Factors such as variations in cortical bone thickness and geometrical features were found to have little effect on the stresses.

Throughout this study, a maximum principal stress criterion was used to evaluate the injury potential of a loading. The validity of such simple concepts for evaluating the strength of complex biological structure may be limited. However, only experimental data of this type is presently available. In view of the many uncertainties in the pilot ejection problem, this does not appear to be a crucial shortcoming. If models of this type agree reasonably well with injury statistics as to the anatomical distribution and likelihood of injury, they will serve as a useful evaluative tool for design and analysis.

The objective of the simplified models is to provide a measure of injury potential which can be used in conjunction with biodynamic models of the spine to predict the likelihood of injury in pilot ejection or other emergency flight procedures. However, these studies have shown that the stress magnitudes predicted by the simplified models are not consistent with the actual stress distributions because of the complexity of the load transmission in the vertebral body. To achieve consistency, either stress reduction factors based on finite element models or alternative simple models will need to be developed.

## APPENDIX

The fundamental natural frequency of the L1 vertebra was estimated using the idealized vertebral model illustrated in Fig. 3, with the assumption that sections remain plane. The classical solution for longitudinal vibration of a continuous bar with one end fixed and the other end free is applicable. The expression for the fundamental natural frequency is

$$\omega = \frac{\pi}{2L} \sqrt{\frac{E}{\rho}}$$

where

$$\begin{aligned} E &= \text{effective modulus of elasticity} \\ &= (E_o(r_o^2 - r_i^2) + E_i r_i^2) / r_o^2 \\ &= 7.54 \times 10^4 \text{ psi} \end{aligned}$$

Note: values for the radii and moduli are

$$\begin{aligned} r_o &= 0.799 \text{ in.} \\ r_i &= 0.787 \text{ in.} \\ E_o &= 2.18 \times 10^6 \text{ psi} \\ E_i &= 1.07 \times 10^4 \text{ psi} \end{aligned}$$

$$\begin{aligned} \rho &= \text{density of water} \\ &= 9.35 \times 10^{-5} \text{ lb-sec}^2/\text{in}^4 \end{aligned}$$

$$\begin{aligned} L &= \text{Length} \\ &= 1.04 \text{ in.} \end{aligned}$$

Evaluation of the expression yields a frequency of 6826 Hertz.

## REFERENCES

- Andriacchi, T.P., Galante, J., Belytschko, T., and Hampton, S., (1976), "A Stress Analysis of the Femoral Stem in Total Hip Prosthesis," J. Bone Jt. Surg. 58 A, 618-624.
- Belytschko, T., Kulak, R.F., Schultz, A.B., and Galante, J.O., (1974), "Finite Element Stress Analysis of an Intervertebral Disc," J. of Biomechanics 7, 277-285.
- Belytschko, T., Schwer, L., and Schultz, A.B., (1976), A Model for Analytic Investigation of Three-Dimensional Head-Spine Dynamics, AMRL-TR-76-10 (ADA-02511), Aerospace Medical Research Laboratory, Wright-Patterson Air Force Base, Ohio.
- Burstein, A.H., Currey, J.D., Frankel, V.H., and Reilly, D.T., (1972), "The Ultimate Properties of Bone Tissue: The Effects of Yielding," J. Biomechanics 5, 35-44.
- Hakim, N.S., King, A.I., (1979), "A Three Dimensional Finite Element Dynamic Response Analysis of a Vertebra with Experimental Verification," J. of Biomechanics 12, 277-292.
- Kazarian, L., von Gierke, H.E., and Mohr, G.C., (1968), "Mechanics of Vertebral Body Injury as a Result of G<sub>z</sub> Spinal Impact," 29th Meeting of Aerospace Medical Association, Bal Harbour, Florida.
- Kazarian, L. (1975), "Standardization and Interpretation of Spinal Injury Criteria and Human Impact Accelerations Tolerance," in Aircraft Crashworthiness, ed. by K. Saczliski, et al, University Press of Virginia, Charlottesville, 153-173.
- Kazarian L., and Graves, G.A., (1977), "Compressive Strength Characteristics of the Human Vertebral Centrum," Spine 21, 1-14.
- Kazarian, L., and Kaleps, I., (1979), Personal communication.
- Kulak, R.F., (1974), "A Study of Intervertebral Disc Mechanics by the Finite Element Method," Ph.D. Thesis, University of Illinois at Chicago Circle.
- Kulak, R.F., Belytschko, T., Schultz, A., and Galante, J., (1976), "Nonlinear Behavior of the Human Intervertebral Disc Under Axial Load," J. of Biomechanics 9, 377-386.
- Orne, D., and Liu, Y.K., (1970), "A Mathematical Model of Spinal Response to Impact," J. of Biomechanics 4, 49-71.

Prager, W., and Hodge, P.G., (1951), "Theory of Perfectly Plastic Solids," John Wiley and Sons, New York.

Prasad, P. and King, A.I., (1974), "An Experimentally Validated Dynamic Model of the Spine," J. Appl. Mech., 546-550.

Puschel, J., (1930), "Der Wassergehalt normaler und degenerierter Zwischenwirbelscheiben," Beitr. Path. Anat., Vol. 84, 123-130.

Tarr, R., Lewis, J.L., Ghassemi, F., Sarmiento, A., Clarke, I., and Weingarten, V., "Anatomic 3-D Finite Element Model of the Proximal Femur with Total Hip Prosthesis," Proc. of Int. Conf. on Finite Elements in Biomechanics, Tuscon, Arizona, 1980, 511-525.

Wilson, E.L., "Solid SAP, A Static Analysis Program for Three Dimensional Solid Structures," University of California at Berkeley, Report UC SESM 71-19, Sept. 1971.